Aus der Chirurgischen Klinik
der Medizinischen Fakultät Charité - Universitätsmedizin Berlin

Dissertation

Über die Messung und Systemische Relevanz von Extrazellulärem Nicotinamidadenindinukleotid in Humanem Plasma

On the Measurement and Systemic Relevance of Extracellular Nicotinamide Adenine Dinucleotide in Human Plasma

zur Erlangung des akademischen Grades
Doctor rerum medicinalium (Dr. rer. medic.)

vorgelegt der Medizinischen Fakultät
Charité - Universitätsmedizin Berlin

von

Philipp Brunnbauer
aus Hamburg

Datum der Promotion:
6. März 2020

Contents

Glossary

Acronym	Full Name
ACLF	Acute-on-chronic liver failure
ADH	Alcohol dehydrogenase
ADP	Adenosine diphosphate
ANKI	Adipose tissue-specific NAMPT knockin
ART	ADP-ribosyltransferase
ATP	Adenosine triphosphate
cADPR	Cyclic ADP ribose
CD	cluster of differentiation
Cx	Connexin
DEPC	Diethyldicarbonat water
DILI	Drug-induced liver injury
DNA	Deoxyribonucleic acid
EtOH	Ethanol
Fas	apoptosis antigen 1 or CD95
GPI	Glycosylphosphatidylinositol
HEPES	4-(2-hydroxyethyl)-1-piperazineethanesulfonic acid
HPLC	High-performance liquid chromatography
IFN-γ	Interferon gamma
IL-10	Interleukin 10
LTx	Liver transplantation
MLO-Y4	Murine Osteocyte-like Cell Line
MM	Master Mix

Acronym	Full Name
MS	Multiple sclerosis
MTT	3-(4,5-dimethylthiazol-2-yl)-2,5-diphenyltetrazolium bromide (tetrazolium dye)
NAFLD	Non-alcoholic fatty liver disease
NAMPT	Nicotinamide phosphoribosyltransferase
NAD	Nicotineamide adenine dinucleotide, indicates both, reduced and oxidised forms of NAD.
NAD^+	Oxidised form of NAD.
NADH	Reduced form of NAD.
NMN	Nicotinamide mononucleotide
NPC	Non-parenchymal cells
PARP	poly ADP ribose polymerase
PC	Parenchymal cells
PES	Phenazine Ethosulfate
PHH	Primary human hepatocyte
PMS	Phenazine Methosulfate
POD	postoperative day
P2X7	P2X purinoceptor 7
r-SBFA	Revised simulated body fluid with albumin
SBF	Simulated Body Fluid
SIRT	Sirtuin
SNR	Signal-to-noise-ratio
TEA	Triethanolamine
TCMR	T cell-mediated rejection
TNFα	Tumor necrosis factor α

Abstract

Deutsch – Diese Dissertation dient dazu das relativ neue Forschungsgebiet des systemischen, extrazellulären Nikotinamidadenindinukleotid ($eNAD^+$) zu skizzieren und liefert einen bescheidenen, aber möglicherweise bedeutsamen Beitrag zu dieser neuen wissenschaftlichen Disziplin. Zunächst wird eine zusammenfassende Einleitung der pathologischen, regenerativen und immunmodulatorischen Charakteristika von $eNAD^+$ präsentiert, wobei hier der Zusammenhang mit dem Gap Junction Alpha-1-Protein, auch bekannt als Connexin 43, im Vordergrund steht. Anschließend wird, basierend auf den vorhergehenden Erkenntnissen, eine 'NAD Escape' Hypothese herausgearbeitet, welche die Beteiligung von $eNAD^+$ an pathologischen und regenerativen Leberprozessen, unter besonderen Gesichtspunkten der immunvermittelnden Eigenschaften von $eNAD^+$, postuliert. Diese besagt, dass $eNAD^+$ Leberabstoßungsreaktionen nach Lebertransplantationen unterdrücken kann und einen lebereigenen Abwehrmechanismus darstellt. Im Weiteren wird die Relevanz und Etablierung des Kernstücks dieser Arbeit, ein neuartiger enzymatischer Assay welcher nanomolare Konzentrationen von $eNAD^+$ in humanem Heparinplasma quantifiziert, anhand einer eigenständigen wissenschaftlichen Veröffentlichung vorgestellt. Hierzu werden die Möglichkeiten für eine vertikale Translation der Anwendungszenarien des Assay innerhalb unserer Studiengruppe dargestellt. Letztlich wird die Vision, eine mit $eNAD^+$ behandelbare 3D-Leberkultur zu etablieren, präsentiert. Diese 3D Leberkultur soll die mechanistische Erforschung der systemischen Rolle von $eNAD^+$ im Zusammenhang mit Leberregenerations- und Leberabstoßungsreaktionen und der NAD Escape Hypothese unterstützen. Erste experimentelle Ergebnisse werden neben einem vorläufigen Protokoll aufgezeigt, welches den Weg für einen zukünftigen miniaturisierten Bioreaktor für die 3D-Leberkultur ebnen soll.

English – This thesis serves to outline the relatively new field of research revolving around systemic, or extracellular nicotinamide adenine dinucleotide ($eNAD^+$) and poses a humble yet potentially meaningful contribution towards this novel scientific niche. Firstly, the reader will be presented with an introductory summary on the pathological, regenerative as well as immunomodulatory facets of $eNAD^+$, with special emphasis on one of its close mechanistic accomplices, connexin 43, otherwise known as gap junction alpha-1 protein. Moving on, these insights will then be utilised to carve out the 'NAD Escape' hypothesis, which postulates the involvement of $eNAD^+$ in pathological and regenerative liver processes, under special consideration of the immune-mediating feats of $eNAD^+$, where it mediates liver rejection reactions following total liver replacement therapies. Lastly, the relevance and establishment of this thesis' centerpiece, a novel enzymatic cycling assay, which quantifies nanomolar concentrations of $eNAD^+$ in human heparinised plasma, will be presented using a standalone scientific publication. Concludingly, a vertical translation opportunity of this assay within our study group is given, that is the vision of establishing an $eNAD^+$ treatable 3D liver culture. This 3D liver culture is envisioned to aid mechanistic research into the systemic roles of $eNAD^+$ in the context of liver regeneration and liver rejection reactions and the NAD Escape hypothesis. Initial experimental efforts, as well as a preliminary protocol are described in addition to groundwork that paves the way for a future miniaturised bioreactor housing this 3D liver culture.

Chapter 1

Introduction

1.1 The Extracellular NAD^+ Pool and the Immune System

In recent years, nicotinamide adenine dinucleotide (NAD) research has significantly picked up the pace as the molecule was found to exhibit some remarkable and intricate involvements in various regulatory pathways, such as circadian rhythms, immune signalling, regenerative processes and pathophysiological events. In fact, it is a common cofactor ubiquitous in all living cells, and, as a pyridine dinucleotide, is composed of one nicotinamide containing nucleotide and one nucleotide containing an adenine nucleobase, which are ultimately joined by a pair of bridging phosphate groups. NAD comes in a dichotomous redox pair, with NAD^+ being the oxidised and NADH the reduced variants of NAD, which are in constant dynamic exchange. This is as they are of central importance as energy transferring molecules in the Krebs cycle, beta oxidation and glycolysis, amongst many other cellular processes such as deoxyribonucleic acid (DNA) repair and mitochondrial protein homeostasis[1, 2]. Generally speaking, oxidised molecules such as $eNAD^+$ present as a more energised and thus reactive species, making them more relevant to our research efforts and this thesis.

Albeit the high cellular compartmentalisation, which we can observe on a microscopic level, NAD^+ is found with a distinctly greater prevalence throughout the intracellular compartment, where it has a plethora of different roles[3]. Yet, $eNAD^+$ levels are known to be the result of lytic release from traumatically insulted tissue as well as non-lytic release through pore forming proteins such as gap junction proteins like connexin 43 (Cx43) hemichannels and are hypothesised to act as danger signals, alerting the immune system to potential tissue damage[1, 4, 5]. When it comes to the immunomodulatory characteristics of $eNAD^+$, various study groups have observed its ability to suppress or mediate local inflammatory responses. More specifically, $eNAD^+$, as a substrate, was able to induce murine T cell apoptosis via the GPI-anchored, raft-associated toxin related ecto-enzyme, ADP-ribosyltransferases 2.2 (ART2.2), through catalysing the ADP-ribosylation of cluster of differentiation 8 (CD8) as well as the cytolytic P2X7 purinoceptor at the Arginin125 site[6]. In addition, $eNAD^+$ was found to generate the same P2X7 ADP-ribosylation, through NAD glycohydrolases/ADPR cyclases such as CD38 and CD157, which ultimately caused calcium influx and subsequent membrane pore formation, accompanied by phosphatidylserine exposure, shedding of CD62L and cell shrinkage, culminating in a completed apoptotic cascade[1, 6]. Remarkably, $eNAD^+$ was observed to invoke this apoptotic cascade at just one-hundredth of the concentration than ATP typically does[6]. Besides the profound effect $eNAD^+$ exerts on T cells, a study by Bruzzone et al., 2006, revealed an $eNAD^+$ associated inflation of the intracellular Ca^{2+} concentration and ensuing activation of granulocytes via the enhancement of their chemotactic properties and the generation of superoxide as well as nitric oxide granules[7].

In addition, the hypothesis of the remarkable ability of $eNAD^+$ to regulate Ca^{2+} flux is derived from its natural role as a substrate for CD38 and the functionally related CD157, which cleaves NAD^+ to form cyclic ADP-ribose (cADPR) and nicotinamide, the former of which is a well-recognised second messenger molecule that facilitates intracellular Ca^{2+}-mediated calcium release[8]. As a concluding mechanistic remark, we can observe that ART expression is strictly limited to naïve T cells, offering the conjecture that P2X7 mediated $eNAD^+$-induced apoptosis explicitly targets the unprimed T cell population[1]. Therefore, $eNAD^+$ could prevent the activation of these resting T cells, which could mitigate the risk of an otherwise imminent autoimmune reaction. In addition, this population shift would enable a more specialised and primed T cell group to conquer the immunological site of action, thereby suggesting an immune response augmentation at the hands of $eNAD^+$. Moreover, $eNAD^+$ is uniquely qualified to take the role as an extracellular signalling agent, specifically in the form of a danger signal, for it can be rapidly mobilised from intracellular stores in order to elicit a given response, which can then be equally rapidly terminated by NAD^+ catabolising ecto-enzymes like CD38 or CD157, representing a well balanced and regulated feedback loop.

Regarding the significance of $eNAD^+$ during the course of systemic disease, recently, Tullius et al., 2014, verified that the systemic administration of NAD^+ was not only able to block experimentally induced autoimmune encephalomyelitis induced paraplegia, yet, even more impressively, reversed disease progression by restoring tissue integrity through remyelination and neuroregeneration via the establishment of immune homeostasis owing to $CD4^+$ $IFN\gamma^+$ $IL\text{-}10^+$ T cells[9]. In addition, $eNAD^+$ was demonstrated to bring about regulatory T cell differentiation, enhancing allograft survival in a murine skin transplantation model with implications for the concepts of alloimmunity, graft rejection and inflammatory disease[10]. It was therefore not unexpected to find $eNAD^+$ meddling in the domain of systemic autoimmunity, where it has been shown to be intricately linked to disease pathologies such as multiple sclerosis (MS), the single most common immune-mediated disorder. In fact, $eNAD^+$ levels were shown to decline by at least 50 % compared to healthy controls, whilst NADH levels doubled with a concomitant three-fold reduction in the NAD^+/NADH redox ratio, representing a less oxidation promoting extra- as well as intracellular environment[11]. On a systemic level, the progression of MS is usually accompanied by an ever-increasing state of fatigue, which has been linked to depleted serum $eNAD^+$ concentrations[11]

The aforementioned research findings deliver the scientific rationale and the foundation of our study group's research project, which aims to unravel the role $eNAD^+$ plays in systemic processes such as T cell-mediated rejection (TCMR) following liver transplantation and liver regeneration in the context of liver resection surgery. Having outlined the principles of $eNAD^+$ formation and its involvement in immunoregulatory processes, the reader will hereinafter be presented with other systemic roles that $eNAD^+$ has been uncovered to play. Subsequently, the scientific inclination towards developing a measurement method for $eNAD^+$ in human plasma is given, with the outlook of ultimately developing an experimental infrastructure that allows the mechanistic research of $eNAD^+$ related pathologies and other systemic processes. This infrastructure is envisioned to comprise a novel and long-term 3 dimensional (3D) liver co-culture, encapsulated in a tailor made bioreactor, combined with a newly developed $eNAD^+$ measurement assay.

1.2 The Systemic Role of Extracellular NAD^+ in Pathology

It has long been established that the silent information regulator 2 (Sir2) protein family (sirtuins) exhibit histone deacetylase activities, which are highly dependent upon the concentration of $eNAD^+$, the cellular currency in DNA repair and metabolic processes. Therefore, $eNAD^+$ can be seen indirectly responsible for transcriptional silencing through the regulation of histone deacetylation. Essentially, this provides the missing link to the very chain that connects various metabolic cycles and energy homeostasis to longevity control and ageing in a multitude of complex higher organisms[12].

In addition, mammals exhibit two distinct versions of the enzyme nicotinamide phosphoribosyltransferase (NAMPT), namely an intra- and extracellular NAMPT variant (iNAMPT and eNAMPT, respectively). Fundamentally, NAMPT is the enzyme which synthesises nicotinamide mononucleotide (NMN), a crucial NAD^+ precursor. Commonly, iNAMPT is acetylated in white and brown adipose tissue[12]. However, when iNAMPT is deacetylated at the lysine 53 site by SIRT1, its enzymatic activity is heightened and, as a result, iNAMPT is then secreted by adipose tissue, forming eNAMPT. Following its secretion, eNAMPT was found to remotely control NAD^+ biosynthesis, neural activity in the hypothalamus and ultimately SIRT1 behaviour in a reciprocal manner[13]. Conspicuously, adipose tissue communicates with different tissues throughout the body by means of eNAMPT secretion, orchestrating the spatiotemporal compartmentalisation of systemic $eNAD^+$ through priming its synthesis. Owing to the established involvement of the hypothalamus as a mammalian control centre of ageing, the thinking of adipose tissue serving as the mediator of this control centre follows naturally. Per example, the murine Adipose tissue-specific NAMPT knockin (ANKI) model demonstrated that the overexpression of iNAMPT in adipose tissue promotes a substantial increase in the systemic eNAMPT concentration, and, consequently, elevated hypothalamic NAD^+ levels in turn leading to higher SIRT1 gene expression profiles and ultimately enhanced physical activity, even in response to fasting[13].

During the course of ageing, NAD^+ availability steadily degrades, which could lead to a reduced excretion of eNAMPT in turn translating to a slimming NMN related NAD^+ synthesis in the hypothalamus and a related increase in adiposity[14]. This seems rather logical as reduced levels of systemic $eNAD^+$ resemble a compromised communication between the thalamus (the control centre of ageing) and adipose tissue (its mediator). A case for the pathological decline in NAD^+ levels and subsequent onset of pathophysiological conditions was made in a study conducted on monozygotic twins, revealing that reduced NAD^+/SIRT pathway expression was associated with the onset of obesity, a general inflammatory state, insulin resistance, as well as impaired mitochondrial protein homeostasis[15]. What is more, non-alcoholic fatty liver disease (NAFLD) has been associated with diminished systemic eNAMPT as well as iNAMPT in hepatic tissue, which, remarkably, was rescued from an apoptotic fate *in vitro* through the addition of eNAMPT, precipitating the enzymatic synthesis of NAD^+[16]. These findings clearly demonstrate the delicate nature of the relationship, that is the interaction of NAD^+ and sirtuins. Should this relationship descend into disorder, the communicative link between adipose tissue and the hypothalamus could be disrupted, leading to a functional systemic decline with age, ultimately constricting mammalian lifespan.

1.3 The Rationale Behind Measuring Extracellular NAD^+ in a Systemic Context

Considering our study group's intricate involvement in liver injury, inflammation and disease, the aim of this project was the development of a valid method for the quantification of $eNAD^+$ levels in human plasma in order to study the effects of $eNAD^+$ during liver surgery and regeneration. The two-step cycling assay that uses albumin modified simulated body fluids in order to measure $eNAD^+$ in human heparinised plasma is described hereafter and was established to help undertake the future exploration of our NAD Escape hypothesis, which will be explained shortly. Translationally, it lays the foundation for the exploration of $eNAD^+$ to be employed as a minimally-invasive biomarker for the detection of fibrotic and cirrhotic morphological changes of liver structures, acute-on-chronic liver failure (ACLF) and liver rejection reactions as well as judging the liver's regenerative capabilities. This is as current methods rely on invasive, painful and expensive bioptic methods as the gold standard for the diagnosis and staging of ACLF as well as fibrotic or cirrhotic processes. However, their diagnostic potential is heavily constrained by the high intra-observer variation among pathologists in the staging of specimens. In addition, bioptic liver procedures suffer from numerous potential complications such as bleeding in the liver parenchyma and around the site of the procedure, including hematomas, strong pain and infection around the catheter entry area and ultimately damage to the liver tissue itself. With the potential role of $eNAD^+$ as a new biomarker in mind, a practical method to monitor $eNAD^+$ levels in human plasma could symbolise a risk minimising alternative to the biopsy.

Additionally, having considered the growing scientific curiosity that is revolving around $eNAD^+$, we set out to establish the first affordable, reliable and highly sensitive method to quantify $eNAD^+$ levels in human heparinised plasma using off-the-shelf materials in order to contribute towards the advancement of this promising research area. This is as a significant lack of medical translation towards the study of mechanistic and pathological involvement of $eNAD^+$ in human disease is apparent, since therapeutic effects of $eNAD^+$ have been virtually only studied in animal models. One of the main shortcomings of any animal study trying to uncover potentially therapeutic effects of $eNAD^+$ was their inability to perform $eNAD^+$ dose response studies, correlating administered NAD^+ with the corresponding effect it had on plasma levels of $eNAD^+$. Thus, these studies exhibited an intrinsic disability to evaluate biologically and therapeutically relevant levels of $eNAD^+$, preventing not only the quantification of these potentially beneficial effects, but rendering the translation to in-human studies virtually impossible, for the first in-human use mandates careful dosage planning. For reasons laid out in the following section, current means of quantifying NAD^+ were not capable to measure $eNAD^+$ in human plasma with adequate accuracy or precision.

Current methods aimed at measuring NAD^+ commonly employ compounds that are reduced in metabolically active cells or environments to produce either a colorimetric, bioluminescence or fluorescence signal, like in the US patent held by Misaki et al., 1985 (Patent No: 4,556,634) or the NAD^+/NADH-Glo™ Assay by Promega (Catalog No: G9071). These methods typically involve the correlation of pyridine nucleotides to the formation of chromogenic formazan dies as a direct reduction product of tetrazolium salts or to the fluorometric signal obtained from the reduced form of resazurin, namely resorufin. Said methods encompass either a direct reduction through NAD^+, or, alternatively, an enzymatic reduction through dehydrogenases and reductases. However, the majority of these studies have been conducted to investigate intracellular NAD ($iNAD^+$), whereas the study of $eNAD^+$ has remained largely untouched, which can be attributed to its extremely low concentrations in the low-micromolar range and relatively complex as well as labour intensive extraction procedures such as separation, pre-fractionation and depletion[3].

Regarding the measurement of highly complex samples, high pressure liquid chromatography (HPLC) coupled to mass spectrometry (HPLC-MS) remains the analytical gold standard. However, the HPLC-MS method, too, suffers from long run times, with a minimum of 10 min per sample not uncommon. Usually this can be traced back to the need for the quantification of the whole NAD metabolome, in order to identify the NAD^+ identity[17]. As a general remark, HPLC analysis methods usually require human plasma samples to be

artificially spiked with NAD^+, which, combined with their long run times, makes their application to high throughput screenings impractical. Moreover, the complexity of the sample matrix to be analysed poses a rather insurmountable challenge for HPLC followed by ultraviolet-visible spectroscopic analysis (HPLC-UV). In fact, this can be explained through the common huge variations in total and individual protein (or other metabolite) concentrations, which, without tedious and elaborate separation, pre-fractionation or depletion techniques, can mask the signal of NAD^+ or significantly distort it by means of ionisation suppression[18]. These shortfalls of HPLC based analysis were deemed to render their sensitivity and specificity inadequate to quantify $eNAD^+$ in human plasma for high throughput applications.

We concluded that a cycling assay was, by its nature, extremely well suited for our research purpose, inasmuch as cycling assays exhibit immense signal amplification potential, which was of paramount importance for the measurement of $eNAD^+$, for we learned that its concentration reached down into the low micromolar range[3]. In addition, cycling assays are known to achieve remarkable analyte specificity through the enzymes they employ. The foundations of enzymatic cycling lie in the reactant recycling of the analyte, which is used to overproportionately amplify a redox indicator dye mediated signal, without the need for additional purification or concentration procedures.

Central to this thesis, Brunnbauer and Leder et al., 2018, produced a methodological paper about said $eNAD^+$ assay, titled "The nanomolar sensing of nicotinamide adenine dinucleotide in human plasma using a cycling assay in albumin modified simulated body fluids" published in Scientific Reports[19]. Therein described lies the process from the assay's inception, through its refinement and finally its establishment based on clinically relevant $eNAD^+$ samples, which will be outlined hereafter. The reader is advised, that, although this thesis ought to feature an in-depth method description as well as accounts of experimental work, the published article is, due to its nature as a method paper, virtually unsurpassable in terms of the level of methodological detail it entrails. Moreover, a collaborative effort between the Charité - Universitätsmedizin Berlin and the Ascenion GmbH has resulted in a patent application at the United States Patent and Trademark Office (USPTO) for the above described $eNAD^+$ assay.

Chapter 2

Materials and Method

2.1 Introductory Methodology of the Extracellular NAD^+ Cycling Assay

For our purposes, we achieved a quantification of $eNAD^+$ by means of establishing a two-step cycling assay, employing NAD^+ as the cofactor for the central enzyme alcohol dehydrogenase (ADH, EC1.1.1.1) from Saccharomyces cerevisiae. ADH catalyses the initial reaction, jumpstarting the reactant recycling. We chose ADH due to its remarkable specificity for NAD^+ as a coenzyme[20]. Illustratively, a schematic of the principle behind this cycling assay is presented in Figure 2.1, where the reader can follow the path of the electrons through each of the assay's cycles. Firstly, the NAD^+ dependent ADH catalyses the dehydrogenation of ethanol to form ethanal (acetaldehyde), thereby reducing the coenzyme NAD^+ to NADH. Subsequently, the reduced pyridine nucleotide NADH promptly passes on the received electron to the secondary redox indicator dye, 3-(4,5-dimethylthiazol-2-yl)-2,5-diphenyltetrazolium bromide (MTT), via the primary indicator dye, phenazine methosulfate (PMS), through the upstream coupled reaction. Subsequently, the rate of reduction of MTT, with formazan as its product, could be analysed on the basis of an absorption based colorimetric measurement at a wavelength of 565 nanometer (nm). Finally, the utilisation of NAD^+ standards with known concentrations enabled the construction of a calibration curve, in turn enabling the correlation of NAD^+ concentrations to slopes of the absorption signals (the production rate of formazan), and thus the extrapolation of an unknown concentration of $eNAD^+$ in a sample from the measured signal increase. In fact, NAD^+ constantly cycles between the primary redox indicator dye, PMS, and ADH in such a fashion that each molecule of NAD^+ naturally leads to the generation of an escalated number of the reduced MTT product formazan, thereby boosting the measurable signal. Due to this process, these assays are often referred to as reactant recycling assays.

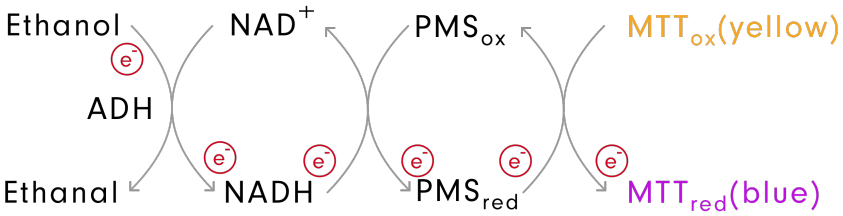

Figure 2.1: NAD^+ cycling illustration. Depiction of the NAD^+ dependent electron transfer from ethanol to ultimately MTT through a two step redox reactant recycling method.

2.2 Deriving a Standard Matrix that Emulates Physiological Conditions

After having derived the $eNAD^+$ signal generating redox cycling reaction, we opted to re-create the most physiological-like standard matrix. When operating enzymatic assays with subsequent sample concentration derivation using calibration curves, it is essential to carry the standards in a surrogate matrix that adequately reflects and resembles the biochemical environment exhibited by heparinised blood plasma, the *in vivo* matrix in which the $eNAD^+$ species resides. This is done to harmonise the reaction dynamics and kinetics of ADH in both, the standard matrix as well as sample matrix. In fact, simply developing a plasma based standard matrix completely free of NAD^+ is unachievable due to this analyte's endogenous nature.

Due to our study group's high involvement in liver resection and liver transplantation procedures, we studied the effect of varying standard matrix albumin concentrations on the assay's predictive capability, the rationale behind this being that patients with pathological liver conditions often present with drastic fluctuations of serum albumin levels. In fact, serum albumin concentration variations are well known on both, an inter- as well as an intrapatient level, especially affecting those suffering from liver cirrhosis. These patients commonly exhibit immensely diminished serum albumin concentrations, as low as 10 g/L, while healthy patients typically present with levels in the range of 35 g/L – 50 g/L. Although the process for finding this standard matrix is presented and discussed in the following sections, the reader is, for the sake of clarity, made aware of the fact that the addition of albumin to the standard matrix has proven crucial in emulating the assay's enzyme kinetics in human plasma.

In order to devise a physiological-like standard matrix, the ionic composition and buffering capabilities of a multitude of commonplace simulated body fluids (SBF) were studied and compared to blood plasma. Ultimately we elected the revised simulated body fluid (r-SBF) to serve as an electrolyte-matched standard matrix for its accurate resemblance of blood plasma's ionic composition. Additionally, it contained HEPES buffer, which features an acid dissociation constant of $p_{ka} = 7.5$, thus more closely resembling the buffering nature of plasma than the otherwise commonly used Tris buffer, exhibiting $p_{ka} = 8.07$[21]. In order to follow our decision making process, the reader is presented with a tabular view of commonly employed SBFs in Table 2.1.

Formulation	Na^+	K^+	Mg^{2+}	Ca^+	Cl^-	HCO_3^-	HPO_4^-	SO_4^-	Buffer
Blood Plasma	142.0	5.0	1.5	2.5	103.0	27.0	1.0	0.5	-
Original SBF	142.0	5.0	1.5	2.5	148.8	4.2	1.0	0.0	Tris
Corrected (c-SBF)	142.0	5.0	1.5	2.5	147.8	4.2	1.0	0.5	Tris
Revised (r-SBF)	142.0	5.0	1.5	2.5	103.0	27.0	1.0	0.5	HEPES
Modified (m-SBF)	142.0	5.0	1.5	2.5	103.0	10.0	1.0	0.5	HEPES

Table 2.1: Commonly used Simulated Body Fluids in comparison to human blood plasma, ionic concentrations are given in (mM).

Finally, r-SBF was adjusted to resemble blood plasma even closer via the addition of albumin (r-SBFA) at a concentration of 40 g/L. Thus, a list of materials used to prepare 1000 ml of a revised simulated body fluid adjusted with albumin (r-SBFA) in DEPC water is given in Table 2.2, below. In fact, varying albumin concentrations of r-SBFA were evaluated with respect to their impact upon the assay performance at 0 g/L (r-SBF), 10 g/L, 20 g/L, 30 g/L and 40 g/L. The prepared r-SBFA was stored in aliquots at −20 °C, until use.

Reagent	Supplier	Amount (g)
BSA	SERVA, GER, Catalog No: 47330.03	40
HEPES	ROTH, GER, Catalog No: 9105.4	11.928
NaCl	SIGMA, USA, Catalog No: 71376	5.403
$NaHCO_3$	SIGMA, USA, Catalog No: S5761	0.740
Na_2CO_3	SIGMA, USA, Catalog No: S7795	2.046
Na_2SO_4	SIGMA, USA, Catalog No: S6547	0.072
KCl	ROTH, GER, Catalog No: 6781.1	0.225
KH_2PO_4	ROTH, GER, Catalog No: 3904.1	0.138
$MgCl_2{\cdot}6H_2O$	ROTH, GER, Catalog No: HN03.1	0.311
$CaCl_2{\cdot}2H_2O$	ROTH, GER, Catalog No: HN04.1	0.388

Table 2.2: List of materials used for the preparation of 1000 mL of a revised simulated body fluid adjusted with albumin (r-SBFA). Approximately 0.8 mL 1.0 N NaOH were used to adjust the pH to 7.5.

2.3 Untangling of the Redox Pair NAD^+ / NADH

Having considered the cycling nature of the assay, one can observe that there are two entry points into the first cyclical reaction. Thus, NADH, the reduced counterpart of NAD^+, too, can enter the reaction directly, bypassing the conversion of ethanol to ethanal, therefore oxidising PMS straight away. Since NADH is present in the extracellular milieu, this would render the independent quantification of $eNAD^+$ unattainable, since one would face an equation containing two unknown variables and merely one measurable constant, a mathematical non-starter. In order to overcome this, we utilised the brilliant method by Lowry et al., 1961, which allowed for a dichotomous, heat-incubation based extraction of the two different pyridine dinucleotides in different pH milieus[22]. In fact, NAD^+ could be isolated from NADH through the addition of a strong acid, here pH 1.5, thereby eradicating virtually all NADH molecules in the sample. Vice versa, the use of a strong base eliminated all NAD^+ molecules, here pH 12.5. After incubation for 10 min at 60 °C, this process guaranteed the independent measurement of both compounds. However, prior to measurement, samples had to be neutralised and shifted back to the physiological working range of ADH, pH 7.4. In order to ensure similar dilution and pH, this process was conducted in parallel on the NAD^+ standards.

2.4 Preparation of the Master Mix

The Master Mix (MM) contained all reagents necessary for the assay apart from the key analyte, $eNAD^+$, residing in the sample to be measured. More precisely, the MM comprised: Alcohol Dehydrogenase from yeast in suspension, (ADH, SIGMA, USA, Catalogue No: 10127558001), thiazolyl blue tetrazolium bromide (MTT, Sigma, USA, Catalogue No: M2128), phenazine methosulfate (PMS, Sigma, USA, Catalogue No: P9625), ethanol (100 %), Triethanolamine (TEA, Sigma, USA, Catalogue No: 90279), and diethyl dicarbonate water (DEPC, Sigma, USA, Catalogue No: D5758). As employed in the MM, the TEA Buffer, stored at room temperature, as well as the ADH solution, stored at 4 °C, were prepared in a ten-fold dilution in DEPC water. Aliquots of PMS and MTT were prepared as 10 mg/mL and 1 mg/mL stock solutions, respectively, and stored at −20 °C. The MM was prepared freshly on ice just prior to measurement to prevent auto-oxidation of PMS and MTT or denaturation of ADH.

In Table 2.3, a list of materials is given, featuring the molar composition of the MM and the respective quantities of the molecules required for a single measurement (150 µL of MM per well). The evaluation of a fluorimetric method was conducted by simply replacing the number of moles of MTT with the same number of moles of resazurin (Sigma, USA, Catalogue No: R7017).

Reagent	Q (µmol)	Well (µL)	Plate (µL)
DEPC	-	41.1	4316
EtOH	129	7.5	788
TEA	25.72	33.6	3528
PMS	0.4	12.3	1292
MTT	0.1	41.4	4347
ADH	125 U	14.4	1512

Table 2.3: List of materials used for the preparation of 150 µL master mix per well, scaled to fit a standard 96 well plate (where 105 wells are considered necessary for the use of a pipetting basin). Note that the reagents employed are the products of this protocol so far, and have thus been previously diluted and weighed into DEPC water.

2.5 Preparation of the NAD Extraction Buffers

In preparation for the sample preprocessing, the NAD^+ and NADH extraction and neutralisation buffers were prepared in DEPC water. Firstly, the NAD^+ extraction buffer consisted of a 0.3 N HCl solution whilst the neutralisation buffer comprised equal parts of 0.36 N TEA-HCl (ACROS, USA, Catalogue No: 170051000) and 0.6 N KOH. Analogously, 0.3 N KOH was used for the NADH extraction buffer. In contrast, the neutralisation buffer was composed of 23 % 0.36 N TEA-HCl, 23 % 0.6 N HCl and 54 % DEPC water.

2.6 Preparation of Standard Solutions

In order to evaluate the assay's linearity, reproducibility and to construct calibration curves, β-NAD (Sigma, USA, Catalogue No: N6522) was utilised as a reaction standard (it is the β–nicotinamide diastereomer of NAD^+, which is found in all organisms). Initially, a 1 mg/mL stock solution of β–NAD was weighed into DEPC water, followed by a 1 : 1000 dilution in DEPC water. Subsequently, the first calibration standard (S1) was obtained by further diluting 500 µL in 500 µL DEPC to achieve a concentration of 0.5 µg/mL (753.6 nM). An additional five serial dilutions constituting 500 µL of previous Standard and 500 µL DEPC water were completed to obtain S2 (376.8 nM), S3 (188.4 nM), S4 (94.2 nM), S5 (47.1 nM) through S6 (23.5 nM), culminating in a total of six calibration standards. Until use, prepared β–NAD aliquots were stored at −80 °C.

2.7 Blood Sample Collection

By means of venipuncture, peripheral venous blood from surgical patients was collected - after having obtained informed consent - into lithium heparin, complying with local regulatory guidelines and the Declaration of Helsinki and approved by the Charité ethics committee (Ethikkommission der Charité Universitätsmedizin Berlin, EA1/291/17 and EA1/018/17). After collection, blood specimen were expeditiously centrifuged at 2500 g for 15 min at 4 °C to separate the plasma compartment from the blood's corpuscular parts. Successively, this plasma was snap frozen in liquid nitrogen and stored in aliquots at −80 °C until being assayed for $eNAD^+$ levels. In addition to our own storage time evaluation, literature provided sufficient evidence that $eNAD^+$ in frozen plasma, as well as the commercially available β-NAD used in this method, were stable for at least three months under these conditions[17].

2.8 NAD Extraction Protocol

As outlined in the preceding sections, we utilised the insights from O'Reilly et al., 2003, to modify the method of Lowry et al., 1961, enabling us to extract $eNAD^+$ and NADH independently[3, 22]. Following venipuncture and the aforementioned described plasma sample processing, heparin plasma samples were, following their collection from the −80 °C freezer and subsequent thawing at room temperature, treated firstly with 0.3 N HCl in order to extract $eNAD^+$. Following this, the administration of 0.3 N KOH was used to extract NADH. For the sake of $eNAD^+$ extraction, initially, 300 µL of plasma sample werte transferred into a new tube. In contrast, 30 µL of plasma sample were transferred to a new tube and supplemented with 270 µL r-SBFA for NADH extraction. Upon addition of the acid and base solutions for pyridine nucleotide extraction, the samples were vortexed and then incubated at 60 °C for 10 min in a heating block. Following heat incubation, the samples were promptly equilibrated on ice for 10 min. Subsequently, the samples were neutralised so as they would feature the optimum working pH of ADH, being 7.4. This was achieved through the addition of 300 µL of their respective neutralisation buffers. The complete procedure was also performed on r-SBFA (later used to supplement the standard solutions and provide their standard matrix).

2.9 Pipetting and Plate Reader Settings

Prior to starting the assay reaction, the MM was prepared and stored on ice. However, no MTT, PMS or ADH were added to the MM at this stage, in order to mitigate auto-oxidation of PMS and MTT as well as denaturation of ADH. Neutralised samples and r-SBFA obtained in the previous section were then centrifuged for 10 min at 16.000 g and 4 °C in order to spin down any microscopic debris. For the samples, 50 µL of the plasma supernatant, complemented with 50 µL of DEPC water (to emulate DEPC used in the β-NAD standard dilutions), were transferred into wells of a transparent multiwell plate. Likewise, 50 µL of standard dilutions S1-S6 were transferred into their respective wells, with each well receiving 50 µL of r-SBFA in addition (to emulate plasma). Generally, all wells were prepared in duplicates for the sake of obtaining duplicate measurements. In order to start assaying, ADH, MTT and PMS were added to the MM, of which 150 µL was then pipetted into every well, resuspending it twice. Subsequently, the plate was stored at room temperature in the dark for 5 min prior to assaying, for ADH to become active. Eventually, the absorbance of the samples was measured at 565 nm in the microplate reader Infinite® 200 PRO (Tecan, Switzerland), with a temperature setting of 25 °C, to prevent significant build-up of bubbles occurring at higher temperatures (with a highly disrupted signal at 37 °C). Generally, all wells were prepared in duplicates and measurements were averaged for the sake of analysis.

2.10 Regression Analysis

Obtained measurements for eNAD$^+$ plasma samples were analysed through the creation of a standard calibration curve, which was, in turn, constructed by fitting an ordinary regression line not through the origin (nTTO, $v_R = mx + v_b$). However, and slightly less common, a regression line through the origin (TTO, $v_R = mx + 0$), proved more robust to an increased albumin related baseline noise, a consequence of the varying albumin concentrations in the standard matrix. Hence, the TTO calibration curve allowed for an albumin independent quantification of eNAD$^+$.

2.11 Reliability, Reproducibility and Linearity

Since this paper's focus lies on the implementation of a novel biochemical measurement technique, one had to evaluate the performance of this new method. In order to satisfy the general scientific requirements we evaluated the repeatability and robustness of the assay, through the quantification of eNAD$^+$ in healthy human heparinised blood plasma in eight independent measurements. Samples were prepared by conducting the thorough and complete preceding experimental protocol, including eight independently prepared standard dilution series, as well as eight separately collected human heparinised plasma samples from a singular, healthy subject. Secondary to the repeatability and robustness examination, these data were further processed to determine the enzyme kinetics of this assay and the resulting interval of linear behaviour.

2.12 Stability of eNAD$^+$ in Long Time Storage

The literature on the stability of eNAD$^+$ in fresh, let alone frozen plasma, is virtually non-existent. However, in order to provide a solid ethical foundation for obtaining and storing blood samples over prolonged periods of time, such knowledge is also crucial for the validity of designed experiments, in particular for the algorithm used to store such samples. With this in mind, we evaluated long-term eNAD$^+$ stability in human heparinised plasma which was stored at $-80\,^\circ$C. For this purpose, we obtained plasma samples from a healthy volunteer and subsequently treated them according to the developed experimental protocol above. Initially, samples were divided into aliquots and eNAD$^+$ was assessed before freezing ($d = 0$), one week after freezing ($d = 7$), as well as one ($d = 30$), two ($d = 60$) and three ($d = 90$) months after freezing.

2.13 Evaluation of a Fluorimetric Alternative

Before the adoption of a colorimetric measurement modality, we explored the ability of a fluorimetric method, for its superior sensitivity and lower limit of quantification, to sense eNAD$^+$ in human heparinised plasma, in consideration of Rhodes et al., 1968[20]. This was readily achieved by replacing MTT in the MM with resazurin, which is reduced by PMS to form the highly red fluorescing resorufin. In order to maintain comparability between fluorimetric and colorimetric techniques, we emphasised the conservation of the number of secondary redox dye molecules (MTT and resazurin) in the MM.

2.14 Statistics

All relevant statistical analysis was conducted using Graphpad's Prism 7 (GraphPad Software, La Jolla, CA, USA). With respect to the evaluation of the $eNAD^+$ storage stability, the method of choice for analysing data was a two-tailed, paired t-test with confidence limits (CL) of CL = 99 %, as well as a two-way ANOVA (without repeated measures) adjusted with Tukey's multiple comparisons test featuring CL = 99 %. The assay's dependence upon the albumin concentration of the standard matrix was evaluated through the implementation of a two-tailed, unpaired t-test with CL = 99 %. When measuring the ratio of neighbouring standard dilution signals, we employed two different methods, namely a simple, two-tailed, unpaired t-test with CL = 99 %, as well as using the more stringent conditions of a two-way ANOVA (without repeated measures) adjusted with Tukey's multiple comparisons test and CL = 99 %. Finally, clinical data was analysed using the nonparametric Mann-Whitney-Wilcoxon test with CL = 95 % for singular time data and the Wilcoxon signed-rank test with CL = 95 % for repeated measures over time, due to relatively small sample sizes (and potential non-normal distribution of the population data). The gold standard method of an ordinary least squares fit was used for regression analysis of the calibration working curve, yielding the Pearson Correlation Coefficient, ρ, as well as the coefficient of determination, R^2 , with CL = 99 %. Overall, a stricter alpha value of $p < 0.01$ was deemed necessary to claim statistical significance for methodological results as opposed the p-value that required for clinical data on $eNAD^+$ plasma concentrations, being $p < 0.05$.

2.15 Flowchart of the Cycling Assay Protocol

Overleaf, in Figure 2.2, the reader is presented with a flowchart of the process of extracting either the reduced or oxidised NAD species, their neutralisation and, ultimately, purification. Additionally, a small summary of the composition of each microwell used during assaying is presented for standard, sample and blank probes.

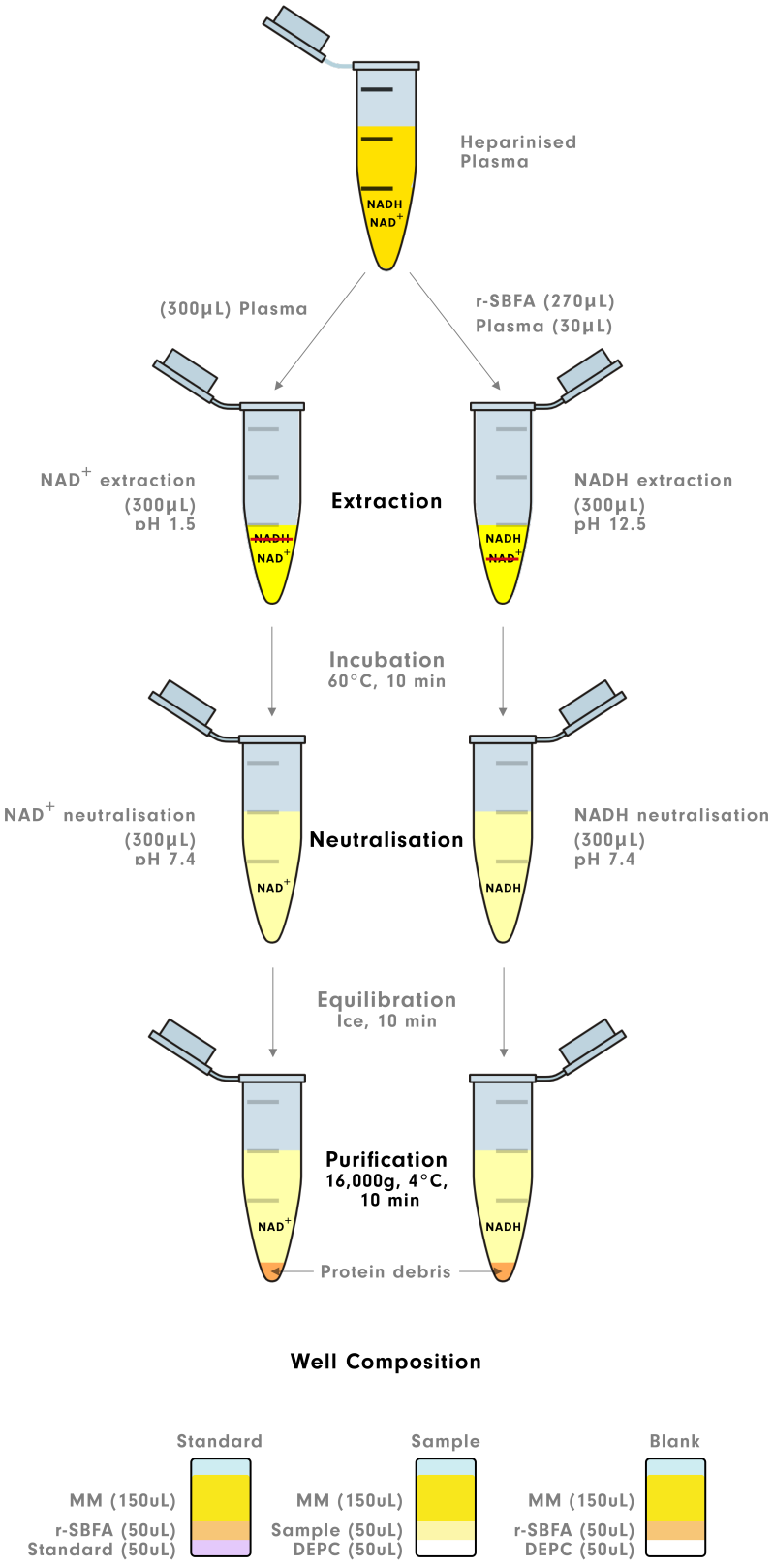

Figure 2.2: NAD^+ cycling assay protocol with an overview of microwell makeups.

Chapter 3

Results

3.1 Results from the Enzymatic NAD^+ Cycling Assay

Essentially, a detailed and thorough examination of the assay's qualitative and quantitative biochemical properties was conducted, including a description of its dynamic as well as temporal resolution in terms of the measurement sensitivity and reproducibility. Initially, results demonstrate the inferiority of a fluorometric, compared to a colorimetric, measurement approach in human plasma. Moreover, an assay calibration procedure, its enzyme kinetics and reaction dynamics were determined, in order to establish the timeframe in which the assay would deliver a constant reaction rate and thus provide valid measurements. Further findings included the discovery of a standard matrix, that would resemble the biochemical properties of human plasma samples in terms of the assay's biochemical behaviour, in order to match the assay's reaction kinetics and dynamics in plasma with the calibration standards. Finally, the publication includes a complete experimental protocol alongside a thorough error propagation analysis and mitigation strategy.

3.1.1 Reaction Dynamics

In order to characterise the reaction dynamics of the initial ADH reaction or rather the formation of formazan, the sample absorbance was measured over the time course of one hour in human heparinised plasma, r-SBFA, DEPC and r-SBF. In fact, the change seen in relative absorbance units (AU) was found highest in human heparinised plasma, with an increase of approximately 1.95 AU over the course of 60 min and 1.84 AU for the runner up, r-SBFA concluded by 1.27 AU and 1.07 AU for DEPC and r-SBF, respectively. The described results are depicted in Appendix B, Figure 1a, and one can clearly observe the r-SBFA curve closely tracking the plasma curve, indicating similar enzyme kinetics in the two different reaction matrices. Additionally, the relative reaction velocities, v_R, in both plasma and r-SBFA were found to be of high resemblance with $v_{RP} = 0.0317 \pm 0.0002$ and $v_{RA} = 0.0306 \pm 0.0002$, respectively. Ultimately, we concluded r-SBFA to be most suited to feature as sample matrix, since it best emulated *in vivo*-like enzyme kinetics of ADH.

Moving on, the optimal time window of the assay was determined through analysing both the slope of the AU trace, represented by the relative reaction velocity, v_R, as well as the slope of the slope, the relative reaction acceleration a_R. Theoretically, v_R should exhibit a linear increase whilst a_R, being the second derivative of the AU trace, should ideally be flat and centred around zero. Examining Appendix B, Figure 3b and 3c, one can observe the relative reaction velocity, v_R, of S1 decreased, adopting a fluctuating and turbulent behaviour after about min 30, with a_R reproducing the adoption of a tumultuous behaviour after roughly min 30 of the assay's reaction. Subsequently, the most well-suited time interval for the quantification of $eNAD^+$ results was deemed to be between min 5 – 25 of the assay reaction.

3.1.2 Colorimetric vs. Fluorimetric Measurement

Having carried out fluorometric and colorimetric measurement methods for eNAD$^+$ analogously, an apparent signal nullification occurring in human heparinised plasma was determined for the fluorometric technique. In order to further explore this surprising finding, being the apparent resorufin signal quenching occurring in heparinised plasma, several autofluorescence scans of the β-NAD standards, plasma samples and the MM were performed. In fact, no signal attenuation was observed in β-NAD standards by themselves. Thus, the autofluorescence spectra of the first β-NAD standard S1 (753.6 nM) was compared to S1 spiked with a small (10 µL) quantity of plasma. Remarkably, the relative fluorescence signal at 590 nm was determined to be 0.964 for S1 and 0.102 for the MM, yielding a 945% signal-to-noise-ratio (SNR), which dropped sharply upon the addition of human plasma to 0.614, giving a 602% SNR. This effect clearly demonstrated the superiority of a colorimetric measurement modality in capturing eNAD$^+$ plasma levels and can be observed in Appendix B, Figure 1c-f.

3.1.3 Linearity and Calibration

Naturally, enzymatic assays exhibit their highest predictive power when they operate within their linear range, meaning that the ratio between the slopes of different standard AU traces should behave in a linear fashion and be equal to the ratio of their respective β-NAD concentrations. The ratios of the first six β-NAD standards were determined to be close to 0.5, thus representing favourable standard β-NAD concentrations, well suited for regression-based analyses. The reader is pointed to Appendix B, Figure 4a for a graphical representation of the findings.

Ultimately, a calibration working curve was constructed using standards S1 through S6 with the TTO method and is presented in Appendix B, Figure 6c. Algebraic analyses revealed a Person correlation coefficient of $\rho = 0.9984$ and the coefficient of determination to be $R^2 = 0.9969$, with the corresponding slope of the calibration curve being $m = (1.75 \pm 0.04)\text{ngAUmL}^{-1}\,\text{min}^{-1}$.

3.1.4 Robustness and Repeatability

With the goal of evaluating the repeatability and robustness of the eNAD$^+$ assay, the complete method was independently carried out eight times, with the respective slopes of the standard curves calculated within the interval of min 5 – 25 of the reaction time. The corresponding relative reaction velocities for each β-NAD standard n, v_{Rn} were found to be, in descending order; $v_{R1} = (9.10 \pm 0.28) \times 10^{-4}\text{AU/min}$ for S1 down to $v_{RS8} = (6.84 \pm 0.42) \times 10^{-5}\text{AU/min}$ for S8 and $v_{RB} = (6.18 \pm 0.33) \times 10^{-5}\text{AU}$ for the blank.

Initially eight calibration standards were intended for the construction of an adequate calibration construction curve. However, the use of a two-way ANOVA (without repeated measures), adjusted with Tukey's multiple comparisons test, revealed that there was no significant difference observable between S6 (23.5 nM) and both, S7 (11.8 nM) as well as S8 (23.5 nM). Overall, the analysis of an individual sample that was carried along all of the eight runs resulted in a relative error of $\delta = 8\%$ in the measured eNAD$^+$ concentration.

3.1.5 Storage

The results of the three month storage trial are depicted in Appendix B, Figure 3d, whereby neither the use of a two-tailed, paired t-test with confidence limits of CL = 99 % nor a two-way ANOVA (without repeated measures) adjusted with Tukeys multiple comparisons test featuring CL = 99 % revealed a statistical significance between any of the measured timepoints, with the average concentration featuring (225.9 ± 16.7)nM. This finding indicated that eNAD$^+$ can be considered stable in human heparinised plasma for at least three months at −80 °C.

3.2 Extracellular NAD^+ in Liver Transplantation

In order to analyse the role of $eNAD^+$ in the context of liver surgery, and as an extension of the produced assay, we analysed the plasma levels of the dinucleotide in patients, who were scheduled to receive liver transplantation (LTx) therapy and compared them with the levels of otherwise healthy controls, who were elected for hernioplasty. Out of the $n = 55$ LTx patients who met the study inclusion criteria, we excluded patients with missing baseline data ($n = 11$), discontinuous specimen collection ($n = 8$) and compromised samples ($n = 5$), leaving us with 31 adequate and continuous $eNAD^+$ datasets. Sociodemographically speaking, 21 patients were male and 10 female with a mean age of (52 ± 13) years (range: 27 years – 72 years). The primary diagnoses yielding the indication for LTx were alcoholic cirrhosis of liver (K70.3, $n = 7$), hepatocellular carcinoma (C22.0, $n = 3$), liver transplant failure after prior LTx (T86.42, $n = 3$), cirrhosis of liver due to chronic hepatitis (B19.20, $n = 2$), primary sclerosing cholangitis (K83.0, $n = 2$), primary biliary cirrhosis (K74.3, $n = 2$), secondary biliary cirrhosis (K74.4, $n = 2$), and other causes ($n = 10$). Regarding the hernioplasty subpopulation, we included $n = 10$ patients, 8 of which were male and 2 female, with a mean age of (52 ± 16) years (range: 29 years – 75 years). Identified underlying diseases were inguinal hernia (K40, $n = 7$), epigastric hernia (K43.9, $n = 1$), hiatal hernia (K44, $n = 1$) and umbilical hernia (K42, $n = 1$).

3.2.1 Preoperative Levels of Extracellualr NAD^+ in Hernioplasty and Liver Transplantation

Initially, we began by comparing baseline levels of $eNAD^+$ in LTx and hernioplasty patients, the results of which are depicted in Figure 3.1. We found that LTx patients exhibited significantly higher baseline $eNAD^+$ concentrations of (354.1 ± 73.2)nM (range: 212.6nM – 492.1nM) than their healthy counterparts, who, in turn, displayed baseline $eNAD^+$ concentrations of (305.2 ± 32.2)nM (range: 240.9nM – 342.7nM) at a significance value of $p = 0.0182$.

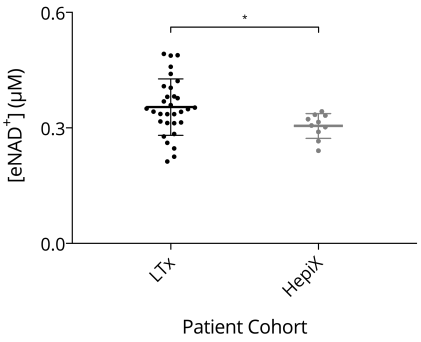

Figure 3.1: Preoperative levels of $eNAD^+$ in patients scheduled to receive liver transplantation or hernioplasty. The overall mean is displayed. **Statistics**: Mann-Whitney-Wilcoxon test with CL = 95 %. A significance level of $p < 0.05$ was applied to reject the null hypothesis. $^*p < 0.05$. All error bars are given in terms of ± SD.

3.2.2 Postoperative Evolution of Plasma Extracellular NAD$^+$ Levels

Secondly, blood specimen of LTx patients were collected prior to the operation (PreLTx) and on the first, third and seventh postoperative day (POD1, POD3 and POD7, respectively). After having assayed said plasma samples for eNAD$^+$ levels, the obtained data was graphed in terms of absolute values on a scatter graph, visualised in Figure 3.2a, as well as relative changes, presented as fold-changes in Figure 3.2b.

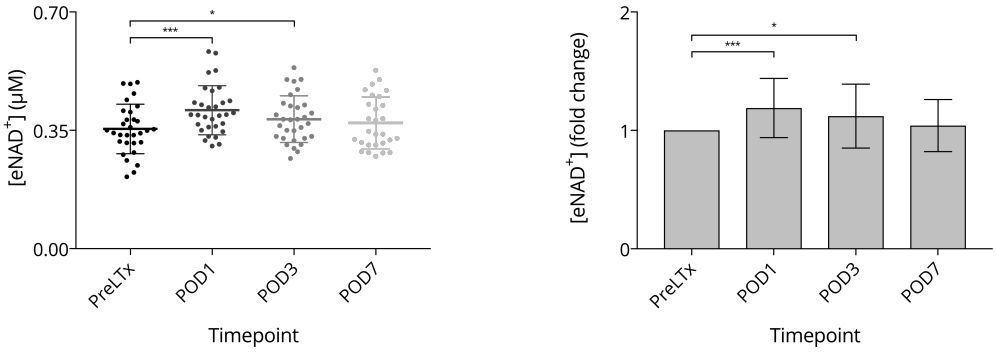

(a) Scatter plot of measured eNAD$^+$ concentrations at baseline and first week after surgery.

(b) Fold-changes of measured eNAD$^+$ concentrations at baseline and first week after surgery.

Figure 3.2: Postoperative evolution of plasma eNAD$^+$ levels in patients who received liver transplantation. Data was gathered preoperative to liver transplantation (PreLTX), and on postoperative days one, three and seven (POD1, POD3 and POD7, respectively). The overall mean is displayed. **Statistics**: Wilcoxon signed-rank test with the confidence limits of CL = 95 %. A significance level of $p < 0.05$ was applied to reject the null hypothesis. $^{***}p < 0.001$ and $^{*}p < 0.05$ All error bars are given in terms of ± SD.

Depicted in Figure 3.2a, and as mentioned above, the preoperative baseline eNAD$^+$ concentration for LTx patients was found to be (354.1 ± 73.2)nM (range: 212.6nM – 492.1nM), which significantly increased to (409.6 ± 72.7)nM (range: 303.8nM – 583.0nM) on POD1 where $p = 0.0002$, and remained significantly elevated on POD3 with a concentration of (383.2 ± 69.3)nM (range: 266.7nM – 535.1nM) and $p = 0.0334$. However, no significantly elevated plasma eNAD$^+$ levels could be experimentally verified on POD 7, given the determined concentration of (372.1 ± 76.7)nM (range: 273.5nM – 527.9nM) had levelled off, returning to baseline concentrations with $p = 0.5331$.

The above findings are further corroborated in the results obtained in an intrapatient analysis of relative, time-dependent eNAD$^+$ plasma level developments, whereby a significant increase to (118 ± 25)% (range: 73% – 185%) of the baseline concentration at POD1 was observed with a significance of $p = 0.0001$. Furthermore, this significant elevation persisted on POD3 with a p-value of $p = 0.0257$ and the concentration being (111 ± 27)% (range: 60% – 191%). Ultimately, a normalisation of eNAD$^+$ levels was ascertained on POD7, with the eNAD$^+$ concentration approaching baseline niveaus at (104 ± 22)% (range: 62% – 159%), resulting in an insignificant difference to the preoperative eNAD$^+$ concentration where $p = 0.4346$.

Chapter 4

Discussion and Future Work

Within the scope of this thesis, a reliable and robust colorimetric two-step enzymatic cycling assay to quantify eNAD$^+$ was established and validated in human heparinised plasma. The assay manages to quantify eNAD$^+$ by means of a two-step enzymatic cycling reaction, based on the initial enzyme ADH. What is more, an albumin modified r-SBF was used to resemble physiological enzymatic activity. In addition, we evaluated assay linearity, reproducibility and confirmed long-term storage stability of eNAD$^+$ in frozen human heparinised plasma.

However, there might well exist various potential sources of error and signal disturbance. Firstly, ADH is known to be modulated in its activity by different hormones, such as growth hormones, epinephrine or estrogens which act in a stimulatory manner, while thyroid hormones and androgens have the potential to inhibit ADH's activity[23, 24]. Thus, varying baseline concentrations of such hormones could contaminate the sample to be measured and impact the ADH used to do so. Yet, this scenario seems to be rather unlikely, as the extraction step (60 °C heat incubation for 10 min at pH 1.5) is expected to denature virtually all proteins and hormones. Continuing with the well known broad specificity of ADH for other aliphatic alcohols, other than ethanol. Per example, ADH is able to oxidise methanol yielding formaldehyde. Methanol is generally not notorious for residing in human blood plasma. Nonetheless, and in part due to dietary preferences for artificial sweeteners such as aspartame methanol can be found with varying concentrations in plasma[25]. In fact, fasting blood levels of methanol were determined to be on average 168μmol/L, which translates to 5.39mg/dL[26]. However, throughout the various stages of the assay samples will experience a 6-fold dilution of methanol levels, resulting in an approximate concentration of 1mg/dL, which is actually less than 1% of the ethanol concentration in the MM (being 125mg/dL). Therefore, the concentration of ethanol, being the key substrate for ADH in the assay reaction, was chosen to lie well beyond the saturation point, in order to outweigh methanol's final sample concentration and suppress any effect it could have on the measured eNAD$^+$ concentration. Taken together, we propose that hormones and other alcohols, endogenous to human blood plasma, will invoke merely negligible effects on the assay's eNAD$^+$ measurement, due to the harsh extraction and neutralisation procedures.

Ultimately, it remains to be mentioned that the correct blood collection method is crucial. In fact, the common chelating agent K3EDTA is known to be a potent inhibitor of ADH, therefore one must always resort to the use of lithium heparin tubes during the acquisition of blood samples[27].

4.1 Paving the Road for Translatory Extracellular NAD^+ Research

In essence, due to it making use of off-the-shelf equipment and requiring no expensive reagents, it can easily be used for high throughput screening of eNAD+ levels in clinical discovery studies. The fact that it has been published under the open access mechanism, makes it basically an open source tool that is free to use and highly time efficient. For instance, the outlined research trend into $eNAD^+$ and its involvement in ageing and obesity could be taken from a speculatory and qualitative to a quantified data domain, boosting the rate of new insights and the discovery of novel potential therapeutic approaches as well as their translational integration.

For instance, it has recently been demonstrated that poly-ADP-ribose polymerase (PARP) appears to be chronically upregulated in the ageing worm and mouse, in turn causing an increase in poly-ADP-ribosylation of cellular proteins[28]. It is hypothesised that this PARP activation could well be the result of elevated and persistent nuclear DNA damage, leading to NAD^+ depletion and consequently a decrease in sirtuin activity, likely contributing to age-associated pathophysiologies. The established $eNAD^+$ assay could play a vital role in driving forward this research.

4.2 The Extracellular NAD^+ Pool and its Involvement in Liver Fibrosis and Rejection

Having outlined the systemic involvement of $eNAD^+$ in the context of ageing, inflammation, disease and immunoregulation, the reader is hereafter presented with a brief introduction of the scientific discoveries outlining the origins of the $eNAD^+$ pool, with special emphasis on hepatic Cx43. In continuation, we will draw parallels between pathological liver processes and Cx43 expression, ultimately speculating on the role of $eNAD^+$ in order to present our NAD escape hypothesis. Often referred to as the goalkeepers of liver homeostasis, connexins appear to be exclusively targeted in pathological processes, justifying their more recent and infamous alias: "pathological pores"[29].

As previously mentioned, $eNAD^+$ is known to form secondary to lytic release, in turn following traumatic tissue injury or non-lytic release facilitated by hemichannels such as Cx43[30]. Intriguingly, the secretory route of Cx43 mediated NAD^+ outflux was subject to long standing scientific controversy and was, in fact, only recently confirmed. The controversy arose from the belief that Cx43 hemichannels, each comprising 6 connexin proteins, would exclusively aggregate in local high density membrane plaques, where they would form gap-junctions with their counterpart hemichannels on juxtaposed cells, in order to form a paracrine signalling conveyor[31]. In addition, no free-floating membrane Cx43 hemichannels (which would then assume the role of membrane pores) were considered to exist, which would have prohibited NAD^+ from leaving the intracellular space, for it would have merely been able to travel from one cell to the next. Although Cx43 expression is usually strictly constrained to the liver's Kupffer cells, hepatocytes have now been identified to exhibit de novo expression of Cx43 in response to hepatotoxic stimuli such as drug-induced liver injury (DILI) facilitated by acetaminophen overdose[32, 33]. In a rodent model, Balasubramaniyan et al., 2013, unravelled that hepatic Cx43 exhibits an increased expression profile during cirrhotic processes, induced through bile-duct ligation surgery as well as following acute-on-chronic liver failure (ACLF), initialised through a lipopolysaccharide treatment[31]. Remarkably, the blocking of Cx43 expression, by means of an anti-Cx43 peptide agent, was associated with a further escalated liver injury with measurably higher hepatocellular necrosis, suggesting that enhanced expression of hepatic Cx43 is linked to inflammation severity and could well be the manifestation of an adaptive, auto-protective response to cirrhotic morphological changes of the liver parenchyma. In fact, this overexpression of Cx43 has also been demonstrated in human cirrhotic liver samples[34].

Having discovered the ability of hepatocytes expressing Cx43 in a de-novo fashion during cirrhotic processes, the reader is presented with mechanistic evidence and consequences of this Cx43 expression in the ensuing section, with special emphasis on the permeability properties of this given connexin. As their hallmark, fibrotic processes lead to the accumulation of extracellular matrix proteins in response to acute or chronic liver injury, and represent the liver's intrinsic wound healing mechanism. A crucial step in the fibrotic remodelling of liver parenchyma is a distinct transformation of stellate cells into a myofibroblast-like phenotype through inflammatory and apoptotic signalling[35]. The liver pathology that is characterised by the most severe and prolonged states of fibrotic change, which in turn lead to nodule formation and grave inhibition of liver function, is referred to as cirrhosis. Cirrhosis is considered an irreversible and devastating condition, leading to end stage liver disease, usually culminating in a fulminant liver failure, with total liver replacement being the therapy of last resort. It has now been firmly established that Cx32 is forfeit in the hepatocyte expression profiles during the transition phase observable in fibrotic hepatic remodelling. In fact, it is replaced with newly synthesised Cx43, and is now considered a hallmark of liver fibrosis[35].

In the pursuit of elucidating the biomechanics of Cx43 and the opening conditions of the membrane pores, Burra et al., 2010, were able to demonstrate that mechanical microstimuli were translated along the glycocalyx of MLO-Y4 cells and primary osteocytes, from both their cell bodies and dendritic processes, resulting in an increased Cx43 opening[36]. Mechanical transduction, therefore, poses a plausible explanation for increased Cx43 mediated iNAD$^+$ release. Combining the knowledge that fibrotic processes are known to meddle with cellular mechanics by elevating tissue stiffness with the fact that liver fibrosis is characterised by cell swelling, in the form of necrotic cell death, one can assume elevated mechanical strain on hepatocytes within the liver parenchyma, leading to an increased iNAD$^+$ release through the above described Cx43 mechanosensing mechanism. Additionally Cx43 was shown to open in response to various pathological stimuli, such as manipulated extracellular or intracellular calcium levels, oxidative stress, ischemia/reperfusion injury and inflammatory states, which are all associated with liver fibrosis[32].

4.3 The NAD Escape Hypothesis and Experimental Evidence

Due to the increasing body of evidence framing eNAD$^+$ as an immunomodulatory agent that is pulling the strings in paracrine and immune signalling via Cx43 hemichannel transport and lytic release, in addition to the above findings, we hypothesise that an increase in eNAD$^+$ acts as an escape mechanism to mitigate cirrhosis mediated cell death as well as rejection reactions, ultimately preventing ACLF or graft failure through TCMR reactions. This process is believed to stem from immune-cell mediated destruction of hepatocytes, which, in turn, lytically release iNAD$^+$ into the extracellular space in addition to their non-lytic release of iNAD$^+$. Especially the latter is expected to play a significant role, mainly facilitated by the de-novo expression of Cx43 on hepatocytes and their subsequently elevated opening probability in pathological conditions due to manipulated extracellular or intracellular calcium levels, oxidative stress conditions, ischemia/reperfusion injury or mechanical microstimuli. It is this eNAD$^+$ that leads to a local inflammatory response suppression through the apoptosis of naïve T cells via the P2X7 receptor, thereby reducing the risk of an autoimmune reaction, as well as an increase in regulatory T cell differentiation, which has been shown to enhance allograft survival rates[1, 10].

In summary, eNAD$^+$ is hypothesised to be of increased presence due to lytic and non-lytic release in cirrhotic processes as well as ACLF, acting as a danger signal which alerts the immune system and liver parenchyma to tissue injury, thereby dampening the local immune response and providing a self-preservation mechanism of the liver graft, which acts to "escape" a liver rejection reaction or cirrhotic process. Experimental evidence of such an escape mechanism has already been uncovered by Okuda et al., 2013, demonstrating an antiapoptotic effect of artificially enhanced eNAD$^+$ levels, whereby NAD$^+$ influx via Cx hemichannels prevented PARP-triggered cortical astrocyte cell death[37]. These findings suggest, that, given the hepatic NAD Escape mechanism proves to exist in future research, it could potentially be manipulated through targeted interventions in the form of systemic eNAD$^+$ supplementation.

Having obtained results of $eNAD^+$ levels in LTx and hernioplasty patients, they can be considered as initial supporting evidence of the NAD Escape hypothesis, the reasoning behind this being two-fold. Firstly, LTx patients seem to exhibit elevated baseline levels of $eNAD^+$ compared to (otherwise healthy) hernia patients, with the concentrations being (354.1 ± 73.2)nM (range: 212.6nM – 492.1nM) and (305.2 ± 32.2)nM (range: 240.9nM – 342.7nM), respectively (Figure 3.1). Using the previous argument, the hypothesis would support these findings in the form of hepatocyte bound de-novo expressed Cx43. Since these patients suffer from severe liver pathologies such as various cirrhosis manifestations, primary sclerosing cholangitis or primary biliary cirrhosis, the hypothesis projects an elevated opening probability of Cx43 in those conditions due to manipulated extracellular or intracellular calcium levels, oxidative stress conditions or cellular mechanical microstimuli. In turn, this would cause more non-lytic release of $iNAD^+$ and thus an elevation of $eNAD^+$. Secondly, the intense surgical trauma in the form of cellular mechanical strain, ischemia/reperfusion injury and an escalated immunologic insult of the graft organ, would most likely cause an even greater $iNAD^+$ release, explaining the greatly increased $eNAD^+$ concentration of (409.6 ± 72.7)nM (range: 303.8nM – 583.0nM) on POD1. However, the falling $eNAD^+$ levels on POD7, returning to baseline at (372.1 ± 76.7)nM (range: 273.5nM – 527.9nM), could be explained through the initial surgical trauma and haemorrhage having started to fade and the immune-escalation being lessened through the establishment of a proper immunosuppressive regimen (for instance through urbason, tacrolimus or everolimus).

4.4 Planning and Establishment of a 3D Liver Co-Culture

In order to facilitate future research efforts into the mechanistic understanding of the involvement of $eNAD^+$ in liver inflammation, disease, regeneration and DILI, our study group aimed to establish a durable *in vivo*-like liver culture, which models regular as well as pathophysiological behaviour of hepatic tissue.

Although an extensive literature review of liver cultures would be beyond the scope of this thesis, having examined novel academic publications and comparing them to current industry standards for the *in vitro* research of hepatotoxicity and liver pathology, one couldn't help but notice a general consensus outlining the inadequacy of current cell culture models, specifically the gold standard, being the primary human hepatocyte (PHH) monolayer culture. Mostly, such arguments were laid out in terms of pharmacokinetic and pharmacodynamic reasoning, where the rapid de-differentiation of PHH alone rendered their ability to study DILI futile. This is as hepatotoxicity studies often require longer time-scales than PHH cultures can satisfy[38]. However, recent achievements in tissue engineering have facilitated the rise of liver-on-a-chip systems as well as organoid cell cultures that often come in the form of spheroids. Arguing the case for PHH spheroid cultures, the reader is presented with their remarkable feats and advantages such as significantly prolonged viability in addition to phenotypic stability, retained morphology, and proteome composition for at least five weeks, easily demonstrating their *in vivo*-like nature and obvious superiority over PHH monolayer cultures, which last merely five to seven days. In fact, the spheroid PHH model was capable of repeatedly demonstrating the *in vivo* hepatotoxic nature of fialuridine at clinically relevant concentrations, which previous monolayer cultures failed to uncover[38]. However, the modulation of monolayer cultures into 3D microtissues, such as spheroids, using either gravity or synthetic scaffolds have been shown to offer a much more *in vivo*-like behaving cell culture, capable of modelling liver function, liver disease and long-term DILI more reliably than the current gold standard and have been shown to reflect pathologies such as cholestasis, steatosis and viral hepatitis. Such cultures can be improved upon even further by containing them in small scale bioreactors or liver-on-chip systems, which feature continuous metabolite monitoring, highly efficient waste disposal and ultimately physiological, rather than pulse like flow conditions (which are non-physiological at a capillary level).

In conclusion, the above presented *in vitro* liver models generally provide either no co-incubation of parenchymal cells (PC) and non-parenchymal cells (NPC) such as hepatic stellate or Kupffer cells, or fail to provide, on a microscopic scale, physiological like tissue scaffolds, for they are often synthetically crafted using inferior manufacturing processes. Therefore, our study group aimed to combine the best of both worlds, the traditional cell culture and an organs-on-a-chip approach. In fact, the co-incubation of PC and NPC on a 3D liver microarchitecture with constant flow bioreactor design was devised, in order to create an *in vivo*-like 3D liver model that can be used to mechanistically assess the NAD Escape hypothesis and unravel the involvement of $eNAD^+$ in liver pathology and regeneration. With this in mind, a preliminary protocol for the *in situ* digestion of the murine liver by a two-step collagenase perfusion followed by the *ex vivo* isolation of parenchymal cells, as well as non-parenchymal cells and their subsequent re-colonisation on a decellularised, cryo-prepared murine liver scaffold, was prepared and is given in Appendix A, Protocol 2. An illustrative flowchart of this protocol is given in Figure 4.1 below and illustrates the liver perfusion, PC and NPC isolation and their eventual re-colonisation on a decellularised liver slice. Said liver slices had been prepared with the kind support of Dr. Hillebrandt and Ms. Daneshgar and are intended to yield the best possible microenvironment for PC and NPC interaction and thus ensure their prolonged viability.

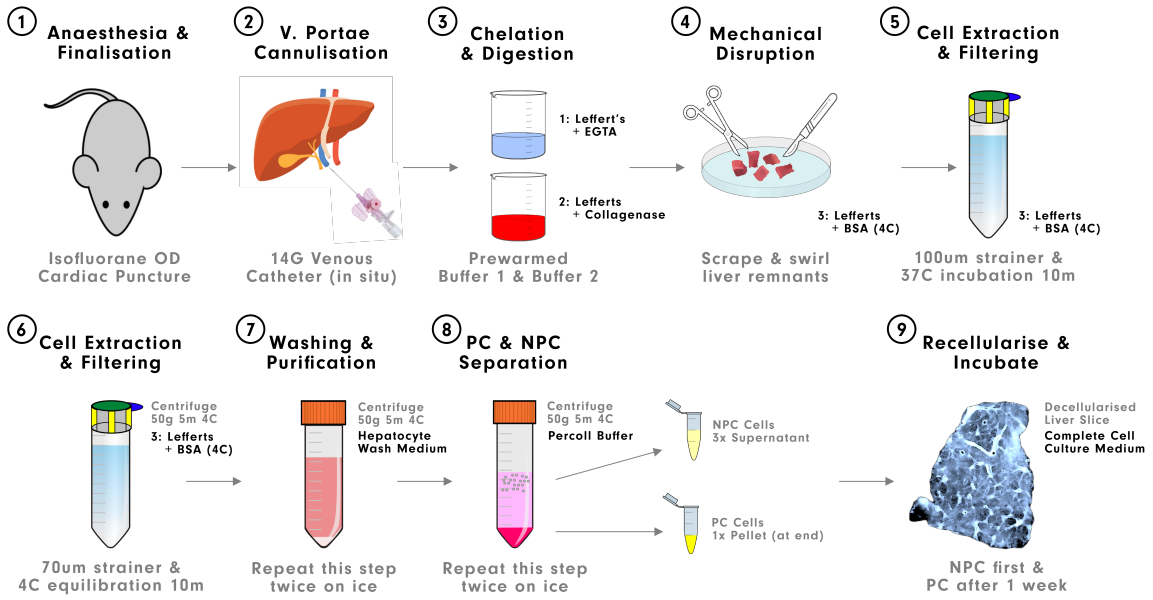

Figure 4.1: Flowchart of the murine liver two-step collagenase perfusion, followed by PC and NPC isolation and their re-colonisation on a decellularised liver scaffold.

After an initial training phase, the PC isolation was successfully performed and PHH were plated on 12-well cell culture plates. The reader is presented with light-microscopic images of the cultured PHH on their third day in culture in Figure 4.2a and of a decellularised murine liver scaffold in Figure 4.2b, courtesy of Dr. Hillebrandt and Ms. Daneshgar.

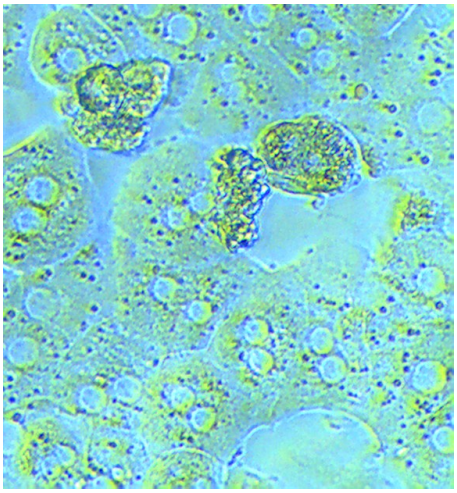

(a) Primary human hepatocyte with $500k$ cells seeded onto a 12-well plate. In two planes: free flowing PHH and adherent PHH were observed.

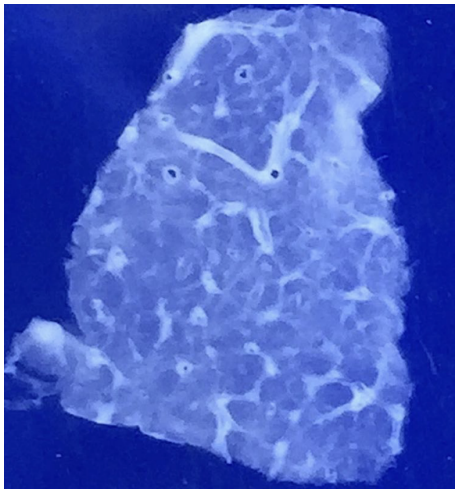

(b) Decellularised liver scaffold, obtained from a murine liver, as it will be used to co-cultivate PC and NPC in the bioreactor.

Figure 4.2: Light microscopic imagery of isolated and plated primary human hepatocytes as well as a decellularised murine liver slice, obtained within the scope of the liver perfusion protocol in Appendix A, Protocol 2.

Based on 3D printing techniques, with SLA being most appropriate, a reusable bioreactor was designed using Autodesk's Fusion 360 (San Rafael, CA, USA) and costs about 20 EUR per piece to manufacture. Renders of the bioreactor are presented in closed configuration in Figure 4.3a and with the lid opened in Figure 4.3b. In addition, images of the manufactured version are given in Figure 4.4a and 4.4b. Naturally, both Luer locks on the side of the reactor would function as the inlet and outlet of the cell culture medium. The liver slice is intended to be held in place by two extending L-arms at the bottom of the lid while the top Luer lock would serve atmospheric generation and drug administration. In fact, the design of the meshes was inspired to facilitate laminar flow conditions through eliminating turbulences caused by the inlet inward-opening shape. Future steps will include transferring the culture to the liver slice and merging it with the described NPC co-incubation, which should occur one week before PC seeding. Finally, the liver slices can then be cultivated in the described bioreactor.

Potentially, this 3D liver culture could be used to simulate surgical trauma, acute TCMR reactions and fibrotic remodelling of the liver parenchyma through the induction of apoptotic, necrotic or necroptotic processes. In order to induce hepatocyte apoptosis, a number of different options seem conceivable, including staurosporine mediated caspase 3 activation or TNFα as well as Fas/CD95 ligand animated procaspase 8 cleavage[2, 39]. Consequently, the NAD Escape hypothesis could be investigated by means of suppressing the non-lytic release of NAD^+ to the extracellular millieu via a Cx43 channel blockage - or rather inhibition - induced by ioxynil, ioxynil octanoate, or, ultimately through a murine knock-out model[40]. Intriguingly, Pittelli2011 demonstrated that the exposure of primary cell lines to eNAD, through transmembrane transport, was able to rescue them from staurosporine-induced apoptosis, mediated by mitochondrial membrane potential loss and ensuing caspase activation[2].

(a) Closed version of the bioreactor where the top Luer lock can be used to administer drugs.

(b) Open version of the bioreactor with the mesh and the L-arms clearly visible.

Figure 4.3: Render of the second iteration of the liver culture perfusion reactor.

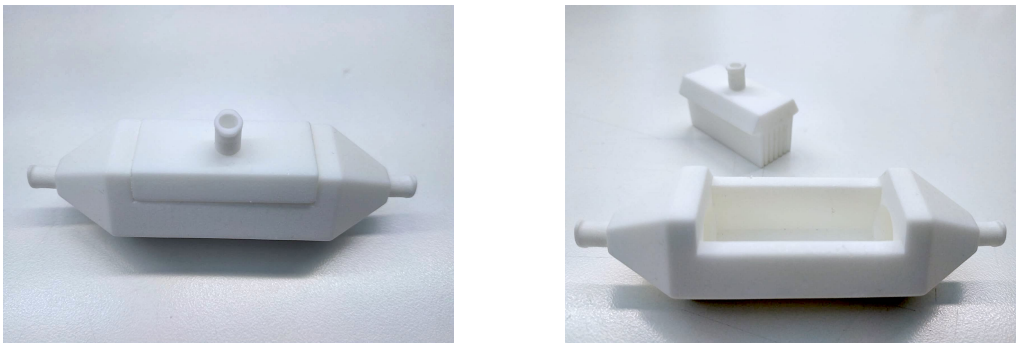

(a) 3D printed version of the bioreactor closed.

(b) 3D printed version of the bioreactor opened.

Figure 4.4: SLA printed version of the second iteration of the liver culture perfusion reactor.

References

[1] F. Haag, S. Adriouch, A. Braß, C. Jung, S. Möller, F. Scheuplein, P. Bannas, M. Seman, and F. Koch-Nolte, "Extracellular NAD and ATP: Partners in immune cell modulation." *Purinergic Signalling*, vol. 3, no. 1, pp. 71–81, 2007.

[2] M. Pittelli, R. Felici, V. Pitozzi, L. Giovannelli, E. Bigagli, F. Cialdai, G. Romano, F. Moroni, and A. Chiarugi, "Pharmacological effects of exogenous NAD on mitochondrial bioenergetics, DNA repair, and apoptosis." *Molecular Pharmacology*, vol. 80, no. 6, pp. 1136–1146, 2011.

[3] T. O'Reilly and D. F. Niven, "Levels of nicotinamide adenine dinucleotide in extracellular body fluids of pigs may be growth–limiting for actinobacillus pleuropneumoniae and haemophilus parasuis." *Canadian Journal of Veterinary Research*, vol. 67, no. 3, pp. 229–231, 2003.

[4] E. R. Lazarowski, R. C. Boucher, and T. K. Harden, "Mechanisms of Release of Nucleotides and Integration of their Action as P2X– and P2Y–Receptor Activating Molecules." *Molecular Pharmacology*, vol. 64, no. 4, pp. 785–795, 2003.

[5] S. Adriouch, W. Ohlrogge, F. Haag, F. Koch-Nolte, and M. Seman, "Rapid Induction of Naive T Cell Apoptosis by Ecto–Nicotinamide Adenine Dinucleotide: Requirement for Mono(ADP–Ribosyl)Transferase 2 and a Downstream Effector." *The Journal of Immunology*, vol. 167, no. 1, pp. 196–203, 2001.

[6] M. Seman, S. Adriouch, F. Scheuplein, C. Krebs, D. Freese, G. Glowacki, P. Deterre, F. Haag, and F. Koch-Nolte, "NAD–Induced T Cell Death: ADP–Ribosylation of Cell Surface Proteins by ART2 Activates the Cytolytic P2X7 Purinoceptor." *Immunity*, vol. 19, no. 4, pp. 571–582, 2003.

[7] S. Bruzzone, I. Moreschi, L. Guida, C. Usai, E. Zocchi, and A. De Flora, "Extracellular NAD+ regulates intracellular calcium levels and induces activation of human granulocytes." *The Biochemical journal*, vol. 393, no. 3, pp. 697–704, 2006.

[8] V. Berthelier, J.-M. Tixier, H. Muller-Steffner, F. Schuber, and P. Deterre, "Human CD38 is an authentic NAD(P)+ glycohydrolase." *Biochemical Journal*, vol. 330, no. 3, pp. 1383–1390, 1998.

[9] S. Tullius, H. R. C. Biefer, S. Li, A. Trachtenberg, K. Edtinger, M. Quante, F. Krenzien, H. Uehara, X. Yang, H. Kissick, W. Kuo, I. Ghiran, M. De La Fuente, M. Arredouani, V. Camacho, J. Tigges, V. Toxavidis, R. El Fatimy, B. Smith, A. Vasudevan, and A. Elkhal, "NAD+ protects against EAE by regulating CD4+ T cell differentiation." *Nature Communications*, vol. 5, pp. 1–17, 2014.

[10] A. Elkhal, H. Rodriguez Cetina Biefer, T. Heinbokel, H. Uehara, M. Quante, M. Seyda, J. M. Schuitenmaker, F. Krenzien, V. Camacho, M. A. de la Fuente, I. Ghiran, and S. G. Tullius, "NAD+ regulates Treg cell fate and promotes allograft survival via a systemic IL–10 production that is CD4+ CD25+ Foxp3+ T cells independent." *Scientific Reports*, vol. 6, p. 22325, 2016.

[11] N. Braidy, C. K. Lim, R. Grant, B. J. Brew, and G. J. Guillemin, "Serum nicotinamide adenine dinucleotide levels through disease course in multiple sclerosis." *Brain Research*, vol. 1537, pp. 267–272, 2013.

[12] S.-I. Imai and L. Guarente, "It takes two to tango: NAD+ and sirtuins in aging/longevity control." *Npj Aging And Mechanisms Of Disease*, vol. 2, p. 16017, 2016.

[13] M. J. Yoon, M. Yoshida, S. Johnson, A. Takikawa, I. Usui, K. Tobe, T. Nakagawa, J. Yoshino, and S.-I. Imai, "SIRT1-mediated eNAMPT secretion from adipose tissue regulates hypothalamic NAD+ and function in mice." *Cell metabolism*, vol. 21, no. 5, pp. 706–717, 2015.

[14] A. Satoh, C. S. Brace, N. Rensing, and S.-I. Imai, "Deficiency of Prdm13, a dorsomedial hypothalamus-enriched gene, mimics age-associated changes in sleep quality and adiposity." *Aging Cell*, vol. 14, no. 2, pp. 209–218, 2015.

[15] S. Jukarainen, S. Heinonen, J. T. Rämö, R. Rinnankoski-Tuikka, E. Rappou, M. Tummers, M. Muniandy, A. Hakkarainen, J. Lundbom, and N. Lundbom, "Obesity is associated with low NAD+/SIRT pathway expression in adipose tissue of BMI-discordant monozygotic twins." *The Journal of Clinical Endocrinology*, vol. 101, no. 1, pp. 275–283, 2016.

[16] T. B. Dahl, J. W. Haukeland, A. Yndestad, T. Ranheim, I. P. Gladhaug, J. K. Damås, T. Haaland, E. M. Løberg, B. Arntsen, K. Birkeland, K. Bjøro, S. M. Ulven, Z. Konopski, H. I. Nebb, P. Aukrust, and B. Halvorsen, "Intracellular Nicotinamide Phosphoribosyltransferase Protects against Hepatocyte Apoptosis and Is Down-Regulated in Nonalcoholic Fatty Liver Disease." *The Journal of Clinical Endocrinology & Metabolism*, vol. 95, no. 6, pp. 3039–3047, 2010.

[17] X. Liang, L. Yang, A. R. Qin, J. Ly, B. M. Liederer, K. Messick, S. Ma, M. Zak, P. S. Dragovich, B. J. Dean, C. E. Hop, and Y. Deng, "Measuring NAD+ levels in mouse blood and tissue samples via a surrogate matrix approach using LC–MS/MS." *Bioanalysis*, vol. 6, no. 11, pp. 1445–1457, 2014.

[18] "Targeted, LCMS-based metabolomics for quantitative measurement of NAD+ metabolites."

[19] P. Brunnbauer, A. Leder, C. Kamali, K. Kamali, E. Keshi, K. Splith, S. Wabitsch, P. Haber, G. Atanasov, L. Feldbrügge, I. Sauer, J. Pratschke, M. Schmelzle, and F. Krenzien, "The nanomolar sensing of nicotinamide adenine dinucleotide in human plasma using a cycling assay in albumin modified simulated body fluids." *Scientific Reports*, vol. 8, no. 1, p. 16110, 2018.

[20] M. J. C. Rhodes and L. S. C. Wooltorton, "A new fluorimetric method for the determination of pyridine nucleotides in plant material and its use in following changes in the pyridine nucleotides during the respiration climacteric in apples." *Phytochemistry*, vol. 7, pp. 337–353, 1968.

[21] A. Oyane, K. Onuma, A. Ito, H.-M. Kim, T. Kokubo, and T. Nakamura, "Formation and growth of clusters in conventional and new kinds of simulated body fluids." *Journal of Biomedical Materials Research*, vol. 64, pp. 339–348, 2003.

[22] O. Lowry, J. Passonneau, and M. Rock, "The stability of pyridine nucleotides." *The Journal of Biological Chemistry*, vol. 236, no. 10, pp. 2756–2759, 1961.

[23] E. Mezey, J. J. Potter, and A. M. Diehl, "Depression of Alcohol Dehydrogenase Activity in Rat Hepatocyte Culture by Dihydrotestosterone," *Biochemical pharmacology*, vol. 35, no. 2, pp. 335–339, 1986.

[24] G. Rachamin, J. A. Macdonald, S. Wahid, J. J. Clapp, J. M. Khanna, and Y. Israel, "Modulation of Alcohol Dehydrogenase and Ethanol Metabolism by Sex Hormones in the Spontaneously Hypertensive Rat. Effect of Chronic Ethanol Administration," *Biochemical Journal*, vol. 186, no. 2, pp. 483–490, 1980.

[25] L. D. Stegink, M. C. Brummel, K. McMartin, G. MartinAmat, L. J. Filer Jr, G. L. Baker, and T. R. Tephly, "Blood Methanol Concentrations in Normal Adult Subjects Administered Abuse Doses of Aspartame," *Journal of Toxicology and Environmental Health, Part A Current Issues*, vol. 7, no. 2, pp. 281–290, 1981.

[26] Y. L. Dorokhov, T. V. Komarova, I. V. Petrunia, V. S. Kosorukov, R. A. Zinovkin, A. V. Shindyapina, O. Y. Frolova, and Y. Y. Gleba, "Methanol may Function as a Cross-Kingdom Signal," *PLoS One*, vol. 7, no. 4, p. e36122, 2012.

[27] J. Dudka, F. Burdan, J. Szumilo, E. Tokarska, A. Korobowicz, R. Klepacz, R. Gieroba, B. Madej, and E. Korobowicz, "Effect of selected alcohol dehydrogenase inhibitors on human hepatic lactate dehydrogenase activity – an in vitro study." *Journal of Applied Toxicology*, vol. 25, no. 6, pp. 549–553, 2005.

[28] L. Mouchiroud, R. H. Houtkooper, N. Moullan, E. Katsyuba, D. Ryu, C. Cantó, A. Mottis, Y.-S. Jo, M. Viswanathan, K. Schoonjans *et al.*, "The NAD+/sirtuin pathway modulates longevity through activation of mitochondrial UPR and FOXO signaling." *Cell*, vol. 154, no. 2, pp. 430–441, 2013.

[29] E. Decrock, M. Vinken, E. De Vuyst, D. V. Krysko, K. D'Herde, T. Vanhaecke, P. Vandenabeele, V. Rogiers, and L. Leybaert, "Connexin–related signaling in cell death: to live or let die?" *Cell Death and Differentiation*, vol. 16, no. 4, pp. 524–536, 2009.

[30] S. Bruzzone, L. Guida, E. Zocchi, L. Franco, and A. De Flora, "Connexin 43 hemi channels mediate Ca2+–regulated transmembrane NAD+ fluxes in intact cells." *The FASEB Journal*, vol. 15, pp. 10–12, 2000.

[31] V. Balasubramaniyan, D. K. Dhar, A. E. Warner, W.-Y. Vivien Li, A. F. Amiri, B. Bright, R. P. Mookerjee, N. A. Davies, D. L. Becker, and R. Jalan, "Importance of Connexin–43 based gap junction in cirrhosis and acute–on–chronic liver failure." *Journal of Hepatology*, vol. 58, pp. 1194–1200, 2013.

[32] M. Maes, E. Decrock, B. Cogliati, A. Oliveira, P. Marques, M. Dagli, G. Menezes, G. Mennecier, L. Leybaert, T. Vanhaecke, V. Rogiers, and M. Vinken, "Connexin and pannexin (hemi)channels in the liver." *Frontiers in Physiology*, vol. 4, p. 405, 2014.

[33] A. Naiki-Ito, M. Asamoto, T. Naiki, K. Ogawa, S. Takahashi, S. Sato, and T. Shirai, "Gap Junction Dysfunction Reduces Acetaminophen Hepatotoxicity with Impact on Apoptotic Signaling and Connexin 43 Protein Induction in Rat." *Toxicologic Pathology*, vol. 38, no. 2, pp. 280–286, 2010.

[34] M. Hernández-Guerra, Y. Gonzlez-Mndez, Z. de Ganzo, E. Salido, J. García-Pagán, B. Abrante, A. Malagón, J. Bosch, and E. Quintero, "Role of gap junctions modulating hepatic vascular tone in cirrhosis." *Liver International*, vol. 34, no. 6, pp. 859–868, 2014.

[35] M. Vinken, "Gap junctions and non-neoplastic liver disease." *Journal of Hepatology*, vol. 57, no. 3, pp. 655–662, 2012.

[36] S. Burra, D. P. Nicolella, W. L. Francis, C. J. Freitas, N. J. Mueschke, K. Poole, and J. X. Jiang, "Dendritic processes of osteocytes are mechanotransducers that induce the opening of hemichannels." *Proceedings of the National Academy of Sciences*, vol. 107, no. 31, pp. 13 648–13 653, 2010.

[37] H. Okuda, K. Nishida, Y. Higashi, and K. Nagasawa, "NAD+ influx through connexin hemichannels prevents poly(ADP-ribose) polymerase-mediated astrocyte death." *Life Sciences*, vol. 92, no. 13, pp. 808–814, 2013.

[38] C. C. Bell, D. F. Hendriks, S. M. Moro, E. Ellis, J. Walsh, A. Renblom, L. F. Puigvert, A. C. Dankers, F. Jacobs, J. Snoeys, R. L. Sison-Young, N. A. Jenkins, R E and, S. Mkrtchian, B. K. Park, N. R. Kitteringham, C. E. Goldring, V. M. Lauschke, and M. Ingelman-Sundberg, "Characterization of primary human hepatocyte spheroids as a model system for drug-induced liver injury, liver function and disease." *Scientific Reports*, vol. 6, p. 25187, 2016.

[39] M. Vinken, M. Maes, A. G. Oliveira, B. Cogliati, P. E. Marques, G. B. Menezes, M. L. Z. Dagli, T. Vanhaecke, and V. Rogiers, "Primary hepatocytes and their cultures in liver apoptosis research." *Archives of Toxicology*, vol. 88, no. 2, pp. 199–212, 2014.

[40] E. Leithe, A. Kjenseth, J. Bruun, S. Sirnes, and E. Rivedal, "Inhibition of Cx43 gap junction channels by the endocrine disruptor ioxynil." *Toxicology & Applied Pharmacology*, vol. 247, no. 1, pp. 10–17, 2010.

Appendix A

Protocols

The reader is overleaf presented firstly with the protocol to carry out the eNAD$^+$ assay, followed by the two-step liver perfusion and 3D liver culture protocol.

1 Extracellular NAD^+ Assay Protocol

1. **Prepare buffers in DEPC water:**
   (a) Acid Preparation
   0.3 N HCl
   0.6 N HCl
   (b) Base Preparation
   0.3 N KOH
   0.6 N KOH
   (c) Extraction Buffers
   NAD extraction: 0.3 N HCl
   NADH extraction: 0.3 N KOH
   (d) Neutralisation Buffers
   TEA-HCl: 0.36 N TEA-HCL, **adjust pH** to 7.4
   NAD neutralisation: 0.36 N TEA-HCl : 0.6 N KOH (ratio 1 : 1)
   NADH neutralisation: 0.36 N TEA-HCl : 0.6 N HCl : DEPC (ratio 46 : 46 : 108)
   (e) Mastermix (MM) Solutions
   TEA-Buffer: 1 : 10 dilution of TEA, **adjust pH** to 7.4
   ADH: 1 : 10 dilution of ADH suspension
   PMS: 10 mg/mL solution
   MTT: 1 mg/mL solution
   EtOH: use 100 % solution **no DEPC**
2. **Prepare NAD^+ Standard Matrix**
   Prepare r-SBFA in 1000ml DEPC, reagents below, add HEPES first, then proceed in order, **adjust pH** to 7.4.
   (a) **NaCl**: 5.403 g, **$NaHCO_3$**: 0.740 g, **Na_2HCO_3**: 2.046 g
   (b) **KCl**: 0.225 g, **KH_2PO_4**: 0.138 g
   (c) **$MgCl_2 \cdot 6H_2O$**: 0.311 g
   (d) **HEPES**: 11.928 g
   (e) **$CaCl_2 \cdot 2H_2O$**: 0.388 g
   (f) **Na_2SO_4**: 0.072 g
   (g) **BSA**: 40 g
3. **Standard Matrix Preparation**
   Prepare a β-NAD standard dilution series in the following manner.
   (a) Prepare a 1 mg/mL solution of β-NAD in DEPC
   (b) Dilute β-NAD solution 1000 fold (10 µL solution in 9990 µL DEPC)
   (c) Dilute 500 µL in 500 µL DEPC to make standard 1 (**S1**), **repeat according to the table below**:

Standard	β-NAD (nM)	β-NAD (ng/mL)
S1	753.6	50.00
S2	376.8	25.00
S3	188.4	12.50
S4	94.2	6.25
S5	47.1	3.13
S6	23.5	1.56

4. **NAD Assay Procedure**

   (a) Get Heparin Plasma (sample) from $-60\,°C$, thaw at room temperature

   (b) Separate plasma sample for extraction
   Pipette $300\,\mu L$ sample in the eppi for NAD extraction
   Pipette $30\,\mu L$ sample + $270\,\mu L$ r-SBFA in the eppi for NADH extraction

   (c) **P**repare standard matrix for extraction (Blank)
   Pipette $300\,\mu L$ r-SBFA into an eppi

   (d) Extraction
   NAD: add $300\,\mu L$ $0.3\,N$ **HCl**
   NADH: add $300\,\mu L$ $0.3\,N$ **KOH**
   r-SBFA: add $300\,\mu L$ $0.3\,N$ **HCl**

   (e) Incubation
   Incubate eppis at $60\,°C$ for $10\,min$ in an eppi heater

   (f) Equilibration
   Equilibrate eppis **on ice** for $10\,min$,

   (g) Neutralisation
   NAD: add $300\,\mu L$ **NAD Neutralisation Buffer**
   NADH: add $300\,\mu L$ **NADH Neutralisation Buffer**
   r-SBF + A: add $300\,\mu L$ **NAD Neutralisation Buffer**

   (h) Deproteinisation
   Centrifuge eppis at $16.000\,g$ for $10\,min$ at $4\,°C$
   Transfer supernatant into new eppis

   (i) Get a **transparent multiwell plate and prepare wells in duplicates (see below)**
   NAD: $50\,\mu L$ of Sample, **NADH:** $5\,\mu L$ of Sample and $45\,\mu L$ of Blank ($1:10$ Dilution)

   (j) Stop the time, add $150\,\mu L$ MM to wells, **resuspend twice!**

   (k) After $5\,min$, measure at $565\,nm$ in Tecan for $30\,min$, analyse results from $5-25\,min$ (linear range)

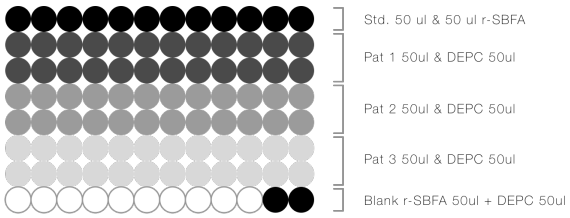

Figure 1: An illustration of a typical multiwell plate layout with β-NAD standards on the top row.

2 3DLiver Culture Protocol

2.1 Chemicals

(a) **Stock Solutions (prepare fresh, use MQ water or a $0.22\,\mu m$ corning filter):**

i. 10x Leffert's Buffer (1 L, sterilised through filtration):
HEPES, 59.57 g (500 mM)
NaCl, 69.27 g (1.15 mM)
KCL, 3.73 g (50 mM)
KH_2PO_4, 1.36 g (10 mM)
pH adjust to 7.4

ii. 1 M $CaCL_2$ (500 mL, sterilised in autoclave):
$CaCl_2 * 2H_2O$, 73.5 g (1 M)

iii. 0.2 M EGTA (500 mL, sterilised through filtration):
EGTA, 38.04 g
Add NaOH to help dissolve

(b) **Perfusion Buffer Solutions (prepare fresh):**

i. Chelation Perfusion Buffer 1 (500 mM):
Leffert's, 50 mM (1x)
EGTA, 1.25 mL(0.5 mM)
Store at 4 °C

ii. Chelation Perfusion Buffer 2 (500 mM):
Leffert's, 50 mM (1x)
1 mM **$CaCl_2$**, 0.5 mL (1 mM)
Collagenase 50 mg
Store at 4 °C

iii. BSA Perfusion Buffer 3 (500 mM):
Leffert's, 50 mM (1x)
1 mM **$CaCl_2$** 1 mL (2 mM)
BSA, 3 g
Store at 4 °C

(c) **Cell Isolation and Culture Solutions:**

i. Hepatocyte Wash Medium (500 mM):
Penicillin/Streptomycin, 5 mL
Store at 4 °C

ii. Complete Culture Medium (500 mM):
Williams' E Medium
FSB 50 g (10 %)
Insulin 100 µL of 100 U/mL (20 mU/mL)
EGF 100 µL of 100 mg/mL (20 ng/mL)
Dexamethasone 0.5 µg (10×10^{-9} M)
Glutamine and antibiotics (Penicillin/Streptomycin) 5 mL)

iii. Attachment Medium (500 mM):
Williams' E Medium
5 % **FSB** 25 mL
Glutamine and antibiotics (Penicillin/Streptomycin) 5 mL)

iv. 0.2 % Gelatin solution (to coate plates, Store at 4 °C):
2 % **gelatin** 55 mL
PBS 500 mL

v. Percoll Buffer:
Hepatocyte wash medium 6 mL (3 parts)
90 % **isotonic Percoll** 2 mL (1 part) - decrease Percoll ration for fatty liver
Prepare just prior to fractionation of cells!

2.2 Liver Perfusion

i. Initialise terminal anaesthesia with a $5\,\mathrm{l/min}$ isoflurane overdose. Once the mouse no longer respond to noxious stimuli, shave and sterilise the abdomen with ethanol and complete finalisation with exsanguination via cardiac puncture with the access point being below the xiphoid (23G needle held in parallel to the spine). Place a paper pillow under the abdomen to facilitate portal vein cannulation.

ii. Enter through a midline incision, dissecting the peritoneum with 4 relief cuts below the extremities, providing maximum exposure of the liver.

iii. Expose the portal vein by using 2 cotton swabs to exenterate the abdominal viscera to the left side.

iv. Pass a sterile 2.0 silk suture underneath the portal vein and tie loosely.

v. Prepare the perfusate tubing by attaching it to the $16-18$G angiocath.

vi. Initiate the ex vivo perfusion with a low flow rate of $1.6\,\mathrm{ml/min}$ of pre-warmed ($37\,^{\circ}\mathrm{C}$) Perfusion Buffer 1, in order to avoid rupturing the portal vein during the insertion of the cannula.

vii. Carefully insert the angiocath into the hepatic portal vein and perfuse in total of $20\,\mathrm{ml}$ at a flow rate of $1.6\,\mathrm{ml/min}$ of Perfusion Buffer 1 (a sign that the cannula is correctly placed inside: the portal vein the liver should instantly begin to blanch resembling a colour shift from dark red to yellow).

viii. Once successful cannulation is confirmed, dissect the inferior vena cava (IVC) to allow efflux and relieve pressure on the portal vein and liver parenchyma. A further test for successful cannulation can be performed by applying light pressure with sterile swab on the IVC; all lobes of the liver should quickly begin to swell. Secure the catheter by closing the surgical knot around the portal vein.

ix. Switch the perfusion solution to Perfusion Buffer 2 (Collagenase) with no interruption of flow for an additional $20\,\mathrm{ml}$ at a flow rate of $1.6\,\mathrm{ml/min}$.

x. Periodically apply pressure with swab to the IVC for $5\,\mathrm{sec}$ intervals ($5-10$ times during digestion). The liver will swell, leading to enhanced hepatic cell dissociation, increasing final yield.

xi. When the liver is digested, (bubbly appearance, very light colour, separation of Glisson's capsule), remove cannula and dissect liver free, place in a pre-chilled sterile beaker with $10\,\mathrm{ml}$ Perfusion Buffer 3. Very carefully resect the gallbladder and subsequently take the liver to tissue cell culture hood.

2.3 Cell Isolation

i. Perform on ice a mechanical disruption of the liver to release hepatocytes. To do this, scrape with tweezers, cannula and swirl the liver in the Perfusion Buffer 3.

ii. Filter the resulting cell suspension through a $100\,\mu\mathrm{m}$ cell strainer into a $50\,\mathrm{ml}$ sterile falcon by the addition of $20-30\,\mathrm{ml}$ of Perfusion Buffer 3

iii. Incubate the filtered cell suspension at $37\,^{\circ}\mathrm{C}$ for $10\,\mathrm{min}$, gently inverting the falcon every $2-3\,\mathrm{min}$.

iv. Equilibrate on ice for $10\,\mathrm{min}$.

v. On ice, filter the suspension with a $70\,\mu\mathrm{m}$ cell strainer into a $50\,\mathrm{ml}$ sterile falcon, fill with Buffer 3.

vi. Centrifuge with $50\,\mathrm{g}$ for $5\,\mathrm{min}$ at $4\,^{\circ}\mathrm{C}$, discard supernatant.

vii. Resuspend in $50\,\mathrm{ml}$ chilled Hepatocyte Wash Medium.

viii. Repeat steps 6 & 7 twice.

ix. Resuspend cells with $5\,\mathrm{ml}$ Percoll Buffer.

x. Centrifuge at $50\,\mathrm{g}$ for $5\,\mathrm{min}$ at $4\,^{\circ}\mathrm{C}$.

xi. SAVE supernatant to obtain NPC in step.

xii. Resuspend cells with $8\,\mathrm{ml}$ Percoll Buffer.

xiii. Centrifuge at $50\,\mathrm{g}$ for 5min at $4\,^{\circ}\mathrm{C}$.

xiv. SAVE supernatant to obtain NPC in step.

xv. Discard the supernatant and resuspend the cells with $10\,\mathrm{ml}$ Attachment Medium.

xvi. Take $10\,\mu\mathrm{l}$ cells and put into $10\,\mu\mathrm{l}$ trypan blue solution to count the cells.

xvii. Plate an appropriate number of cells in Attachment Medium on plates/dishes or rat tail Collagen ($12.5\,\mathrm{mg/cm^2}$).

xviii. Incubate the cells for $2-3\,\mathrm{h}$ or until attachment has occurred.

xix. Remove the medium, rinse gently with PBS or medium to remove unattached cells and replace with fresh Starvation Medium or Complete Culture Medium. Incubate overnight.

xx. Next day, start treatment of the cells using Starvation Medium/Complete Culture Medium and/or harvest.

Appendix B

Publication and Regulatory Documents

B.1 Eidesstattliche Versicherung

"Ich, Philipp Brunnbauer, versichere an Eides statt durch meine eigenhändige Unterschrift, dass ich die vorgelegte Dissertation mit dem Thema: On the Measurement and Systemic Relevance of Extracellular Nicotinamide Adenine Dinucleotide in Human Plasma / Über die Messung und Systemische Relevanz von Extrazellulärem Nicotinamidadenindinukleotid in Humanem Plasma selbstständig und ohne nicht offengelegte Hilfe Dritter verfasst und keine anderen als die angegebenen Quellen und Hilfsmittel genutzt habe.

Alle Stellen, die wöärtlich oder dem Sinne nach auf Publikationen oder Vorträgen anderer Autoren beruhen, sind als solche in korrekter Zitierung kenntlich gemacht. Die Abschnitte zu Methodik (insbesondere praktische Arbeiten, Laborbestimmungen, statistische Aufarbeitung) und Resultaten (insbesondere Abbildungen, Graphiken und Tabellen) werden von mir verantwortet.

Meine Anteile an etwaigen Publikationen zu dieser Dissertation entsprechen denen, die in der untenstehenden gemeinsamen Erklärung mit dem/der Erstbetreuer/in, angegeben sind. För sämtliche im Rahmen der Dissertation entstandenen Publikationen wurden die Richtlinien des ICMJE (International Committee of Medical Journal Editors; www.icmje.og) zur Autorenschaft eingehalten. Ich erkläre ferner, dass mir die Satzung der Charit - Universitätsmedizin Berlin zur Sicherung Guter Wissenschaftlicher Praxis bekannt ist und ich mich zur Einhaltung dieser Satzung verpflichte.

Die Bedeutung dieser eidesstattlichen Versicherung und die strafrechtlichen Folgen einer unwahren eidesstattlichen Versicherung (§§156, 161 des Strafgesetzbuches) sind mir bekannt und bewusst."

Unterschrift und Stempel des erstbetreuenden Hochschullehrers

---

Unterschrift des Doktoranden

B.2 Publication

1: Brunnbauer P*, Leder A*, Kamali C, Kamali K, Keshi E, Splith K, Wabitsch S, Haber P, Atanasov G, Feldbrügge L, Sauer IM, Pratschke J, Schmelzle M, Krenzien F. The nanomolar sensing of nicotinamide adenine dinucleotide in human plasma using a cycling assay in albumin modified simulated body fluids. *Scientific Reports*. 2018; **8**(1): 16110. DOI: 10.1038/s41598-018-34350-6. ***Shared first authorship**.

B.2.1 Individual Work Contribution

As per the doctoral regulations that are in effect as of 1st November 2017 (AMB 199, section 6.4), a shared first authorship shall be accompanied by detailed accounts of the individuals' contribution towards the publication, in order to be accredited by the commission, (AMB 199 §7 section 1/2).

Philipp Brunnbauer

- *Publication contribution*;
  Drafted and finalised manuscript, and
  Compiled and analysed data, and
  Prepared publication figures, and
  Statistical analyses of all results, and
  Calculation of enzyme kinetics of ADH (Figure 4b).
- *Experimental contribution*;
  Establishment of substrate ethanol as opposed to methoxyethanol in previous protocols, and
  Evaluation DEPC water utilisation (Fig 1a), and
  Evaluation of MTT vs resazurin as reaction indicator dye (Figure 1b, c, d, e and f), and
  Evaluation of eNAD$^+$ storage time (Figure 3d), and
  Evaluation of the β-NAD standards (Fig 4a, Fig 6a and b), and
  Refined and finalised assay protocol and timing (Figure 4b and c), and
  Evaluation of albumin's effect on standard reaction kinetics (Figure 5a, b, c and d), and
  Automated NAD concentration calculation from calibration curves (Fig 6c), and
  Measurement of clinical NAD$^+$ samples (Figure 6d), and
  Evaluation of pH shifts during extraction and neutralisation steps (Table 5), and
  Evaluation and determination of plate reader protocol.

Annekatrin Leder

- *Publication contribution*;
  Initial literature review, and
  Drafted manuscript, and
  Prepared publication figures.
- *Experimental contribution*;
  Groundwork laid for enzymatic cycling principle, and
  Resazurin based assay derived initial protocol, and
  General study design, including sample acquisition, preparation and storage.

Unterschrift und Stempel des erstbetreuenden Hochschullehrers

---

Unterschrift des Doktoranden

B.3 European Credit Transfer and Accumulation System (ECTS) Efforts

Further Education

- **US Patent registration at the USPTO**, based on the publication: The nanomolar sensing of nicotinamide adenine dinucleotide in human plasma using a cycling assay in albumin modified simulated body fluids. *Scientific Reports*. 2018; **8**(1): 16110. DOI: 10.1038/s41598-018-34350-6,
- Completed the Stanford University Online: **Statistics in Medicine**,
- Completed the Charité FEM Basic Course on **Laboratory Animal Science (Mouse/Rat)**.

Congress-participations & Presentations

- Forschungs-Colloqium: 02.03.19 - *Presenter & Listener*,
- Eyeforpharma: 12-14.03.19 - *Presenter & Listener*,
- Imperial College Health Hack: 17-18.03.18 - *Supervisor & Presenter*,
- Imperial College Alumni Congress: 30.06.18 - *Presenter & Listener*,
- Conferences at Ahoy!, Wattstrasse 11: Multiple dates - *Presenter, Panelist & Debater*,
- Das deutsche Gesundheitssystem: Innovation = Fortschritt?: 20.06.18 - *Listener*,
- Health-IT-Talk: Medizintechnik und Sicherheit: 13.08.18 - *Listener*,
- Startupbootcamp: 27.11.18 - *Listener*.

Unterschrift des Doktoranden

B.4 Publication and ISI Web of Knowledge Ranking

Based on the extract from the ISI Web of Knowledge, the journal *Scientific Reports* ranked 12 out of 64 Journals in the category "Multidisciplinary Sciences", with an impact factor (2017) of 4.122 and an eigenfactor (2017) of 0.71896, whilst the Journal *Journal of Hepato-Biliary-Pancreatic Sciences* ranked 45 out of 200 in the category "Surgery", with an impact factor (2017) of 2.877 and an eigenfactor (2017) of 0.00713. Data was obtained from `https://intranet.charite.de/medbib/impact_faktoren_2017_fuer_zeitschriften_nach_fachgebieten/` on 17.05.2019 at 12:37 pm. The relevant excerpts are given overleaf.

Journal Data Filtered By: **Selected JCR Year: 2017** Selected Editions: SCIE,SSCI Selected Categories: **"MULTIDISCIPLINARY SCIENCES"** Selected Category Scheme: WoS

Gesamtanzahl: 64 Journale

Rank	Full Journal Title	Total Cites	Journal Impact Factor	Eigenfactor Score
1	NATURE	710,766	41.577	1.355810
2	SCIENCE	645,132	41.058	1.127160
3	Nature Communications	178,348	12.353	0.926560
4	Science Advances	10,194	11.511	0.057080
5	PROCEEDINGS OF THE NATIONAL ACADEMY OF SCIENCES OF THE UNITED STATES OF AMERICA	637,268	9.504	1.108220
6	National Science Review	952	9.408	0.004340
7	GigaScience	1,694	7.267	0.011030
8	Scientific Data	1,567	5.305	0.008550
9	Journal of Advanced Research	1,843	4.327	0.003820
10	Annals of the New York Academy of Sciences	46,160	4.277	0.033270
11	Science Bulletin	1,952	4.136	0.005900
12	Scientific Reports	192,841	4.122	0.718960
13	Journal of the Royal Society Interface	11,357	3.355	0.030960
...				
56	Maejo International Journal of Science and Technology	183	0.469	0.000270
57	SCIENCEASIA	536	0.447	0.000590
58	Chiang Mai Journal of Science	455	0.409	0.000570
59	NEW SCIENTIST	917	0.386	0.001120
60	INTERDISCIPLINARY SCIENCE REVIEWS	238	0.311	0.000080
61	JOURNAL OF THE NATIONAL SCIENCE FOUNDATION OF SRI LANKA	213	0.305	0.000240
62	COMPTES RENDUS DE L ACADEMIE BULGARE DES SCIENCES	570	0.270	0.000410
63	ACTA SCIENTIARUM-TECHNOLOGY	246	0.231	0.000400
64	R&D MAGAZINE	19	0.109	0.000000

SCIENTIFIC REPORTS

OPEN

The nanomolar sensing of nicotinamide adenine dinucleotide in human plasma using a cycling assay in albumin modified simulated body fluids

Received: 30 May 2018
Accepted: 15 October 2018
Published online: 31 October 2018

Philipp Brunnbauer[1], Annekatrin Leder[1], Can Kamali[1], Kaan Kamali[1], Eriselda Keshi[1], Katrin Splith[1], Simon Wabitsch[1], Philipp Haber[1], Georgi Atanasov[1], Linda Feldbrügge[1,2], Igor M. Sauer[1], Johann Pratschke[1], Moritz Schmelzle[1] & Felix Krenzien[1,2]

Nicotinamide adenine dinucleotide (NAD), a prominent member of the pyridine nucleotide family, plays a pivotal role in cell-oxidation protection, DNA repair, cell signalling and central metabolic pathways, such as beta oxidation, glycolysis and the citric acid cycle. In particular, extracellular NAD^+ has recently been demonstrated to moderate pathogenesis of multiple systemic diseases as well as aging. Herein we present an assaying method, that serves to quantify extracellular NAD^+ in human heparinised plasma and exhibits a sensitivity ranging from the low micromolar into the low nanomolar domain. The assay achieves the quantification of extracellular NAD^+ by means of a two-step enzymatic cycling reaction, based on alcohol dehydrogenase. An albumin modified revised simulated body fluid was employed as standard matrix in order to optimise enzymatic activity and enhance the linear behaviour and sensitivity of the method. In addition, we evaluated assay linearity, reproducibility and confirmed long-term storage stability of extracellular NAD^+ in frozen human heparinised plasma. In summary, our findings pose a novel standardised method suitable for high throughput screenings of extracellular NAD^+ levels in human heparinised plasma, paving the way for new clinical discovery studies.

Nicotinamide adenine dinucleotide (NAD) is a pyridine dinucleotide omnipresent in all living cells either in oxidised (NAD^+), or reduced (NADH) form, whose ratio dictates the intracellular redox status and thus stipulates the overall cellular metabolic state[1,2]. Extracellular NAD^+($eNAD^+$) was shown to exhibit important secondary messenger properties and acts to induce intracellular calcium release, thereby mediating lymphocyte chemotaxis[3]. Interestingly, $eNAD^+$ is known to be the result of either lytic release from injured tissue or non-lytic release mechanisms through pore forming proteins like connexin 43 (Cx43) hemichannels and is thus hypothesised to mediate immune response and organ function by means of paracrine signalling[4–6].

Therapeutic applications of $eNAD^+$ have been subject to extensive testing in murine models, with striking findings demonstrating anti-aging, regenerative and highly immunomodulatory traits[7,8]. For instance, Tullius *et al.*[9], discovered that the systemic administration of β-NAD^+ did not only block autoimmune encephalomyelitis induced paraplegia, but reversed disease progression through remyelination and neuroregeneration[9]. Furthermore, $eNAD^+$ induced regulatory T cell differentiation, promoting allograft survival in a murine skin transplantation model with implications for concepts of alloimmunity and inflammatory diseases[10]. However, a significant lack of medical translation towards the study of $eNAD^+$ in human disease is apparent.

In fact, the measurement of $eNAD^+$ in different bodily compartments is challenging due to vast concentration variations. In human erythrocytes, intracellular NAD^+ ($iNAD^+$) was determined to be in the range of 10–40 M, whilst $eNAD^+$ in pig plasma was found at a fraction of this concentrations, namely 240–290 nM[11–13]. Therefore,

[1]Experimental Surgery and Regenerative Medicine, Department of Surgery, Campus Charité Mitte and Campus Virchow-Klinikum, Charité - Universitätsmedizin Berlin, Berlin, 13353, Germany. [2]Berlin Institute of Health (BIH), Berlin, 10178, Germany. Philipp Brunnbauer and Annekatrin Leder contributed equally. Correspondence and requests for materials should be addressed to F.K. (email: felix.krenzien@charite.de)

analytical tests have to be inherently robust and span vastly different concentration ranges. High performance liquid chromatography (HPLC) NAD^+ analysis methods usually require any and all samples to be internally spiked with NAD^+ and have struggled to quantify NAD due to signal masking and ionisation suppression, especially when followed by ultraviolet-visible (HPLC-UV) spectroscopic quantification[14]. However, HPLC methods followed by mass spectrometry (HPLC-MS), and especially tandem mass spectrometry (HPLC-MS/MS), have managed to achieve remarkable sensitivity and specificity for $iNAD^+$ thanks to their ability to separate the respective metabolites through elution with highly specialised columns and successively combining the relaxation time of specific metabolites with their mass spectrum[15]. Generally, the entirety of the apparatus, namely the columns, the mass or UV spectrometer as well as the actual HPLC machine, required for HPLC analyses tends to come with a hefty price tag, rendering it prohibitively expensive for the general scientific community. Typically, each singular measurement of LC-based assays consumes significant amounts of time, from ten minutes up to one hour, making their application to high throughput screenings impractical.

A promising concept enabling the measurement of minuscule analyte concentrations is known as enzymatic cycling, whereby a reactant recycling of the analyte takes place and is used to overproportionately amplify a redox indicator dye mediated signal, without the need for additional purification or concentration steps. First introduced by Warburg *et al.*[16], the analysis of pyridine nucleotides was pioneered through an enzymatic cycling reaction[17–19]. In an effort to refine this method, Rhodes *et al.*[20], used alcohol dehydrogenase for the cycling reaction and quantification of pyridine nucleotides in cox orange apples[20]. Although this method relied on the fluorimetric measurement of the highly red fluorescing resorufin, the reduced form of resazurin, the signal might be masked by the autofluorescence of plasma. In later years, ADH gained popularity and was subsequently adopted as the enzyme of choice, as it is present in all living organisms[21–23]. Nonetheless, the majority of these studies have been conducted to investigate $iNAD^+$, and have not been validated for the study of $eNAD^+$ in human plasma. Consequently, we established a method to meet the challenges of measuring $eNAD^+$ in human plasma based upon known protocols[13,20,24]. More precisely, a heat based dichotomous pH extraction procedure was implemented to extract purified versions of NAD^+ or NADH, subsequently quantified by a colorimetric two-step enzymatic cycling assay[18,25]. The method's sensitivity ranged from the low micromolar into the low nanomolar domain, using an albumin adjusted revised simulated body fluid (r-SBFA) as standard matrix in order to optimise enzymatic activity and to increase assay linearity, providing a matrix closely resembling human plasma. The assay at hand satisfies common analytical standards of linearity, reproducibility and analyte storage stability. Perspectively, this method is intended to meet the present scientific curiosity around and reveal the role of $eNAD^+$ in immunological, oncological and systemic diseases.

Results

Evaluation of standard matrix and spectroscopy method. The standard matrix is one of the most crucial components of any assay, as its aim is to match the enzymatic cycling behaviour in plasma to that in the standards. Therefore it is crucial to the validity of the assaying method. In order to emulate the enzyme kinetics of ADH in human heparinised plasma and to gain assay sensitivity, several standard matrices were compared against human plasma, namely DEPC water, r-SBF and r-SBFA, using β-NAD Standards. Since a standard matrix might not be completely free of analyte, and, since human plasma endogenously features $eNAD^+$, every standard matrix was accompanied by blanks produced from the same matrix. The resulting absorbance unit (AU) readings are presented in Fig. 1a, where all matrices were spiked with 50 µL of β-NAD standard S2 (376.8 nM). A qualitative inspection revealed that r-SBFA and heparinised plasma both presented with a highly linear increase, whereas DEPC and r-SBF. The absorbance increase reflects the enzyme velocity of ADH, and was highest in human heparinised plasma, with an increase of approximately 1.95 AU over the course of 60 min and 1.84 AU for the runner up, r-SBFA, concluded by 1.27 AU and 1.07 AU for DEPC and r-SBF, respectively. Analogously, the relative reaction velocity, v_R, in plasma and r-SBFA were of remarkable resemblance, namely $v_{RP} = 0.0317 \pm 0.0002$ and $v_{RA} = 0.0306 \pm 0.0002$, respectively. All things considered, we found r-SBFA to best emulate *in vivo*-like enzyme kinetics of ADH, therefore adopting it as the standard matrix.

The advantages of fluorimetric over colorimetric detection techniques are well known and include a higher sensitivity and specificity as well as a lower limit of detection. Therefore, we evaluated whether a fluorimetric method was superior to the colorimetric method. For this purpose, MTT was used for absorbance and resazurin for fluorescence, both representing the signal generating molecules. Since the signal of interest arises from the fluorophore ejection from resorufin at a wavelength of 590 nm, an autofluorescence scan of both, the master mix (MM) and a human heparinised plasma sample was performed and a close-up view is given in Fig. 1b. Indeed, the relative autofluorescence spectra of the MM and plasma sample were found to differ only marginally from approximately 0.093 for the $eNAD^+$ plasma sample and 0.057 for the MM, yielding a signal to noise ratio (SNR) of 163%. The measured fluorescence unit (FU) and absorbance unit (AU) readings for β-NAD standards and human plasma are depicted in Fig. 1c,d. Despite the obvious parallelism of the colorimetric and fluorimetric standard traces of β-NAD at different concentrations, the reader is pointed to the apparent nullification of the fluorescence plasma signal. In contrast, the colorimetric detection method exhibited a strong signal for human plasma. In order to elucidate this surprising finding, that is, the apparent resorufin signal quenching in plasma, several autofluorescence scans of the β-NAD standards, plasma samples and mastermix (please see methods) were conducted and are given in 1e and 1f. We further explored the fact that a signal was obtainable from the β-NAD standards, yet virtually absent from all plasma samples by comparing the autofluorescence spectra of the first β-NAD standard S1 (753.6 nM) to S1 spiked with a small (10 µL) quantity of plasma. Strikingly, the relative fluorescence signal at 590 nm was found to be 0.964 for S1 and 0.102 for the MM (945% SNR), which dropped sharply upon the addition of human plasma to 0.614, giving a 602% SNR. Note, the first emission spike around 320 nm from formulations containing either albumin or plasma is in fact due to the autofluorescence of albumin itself, since its

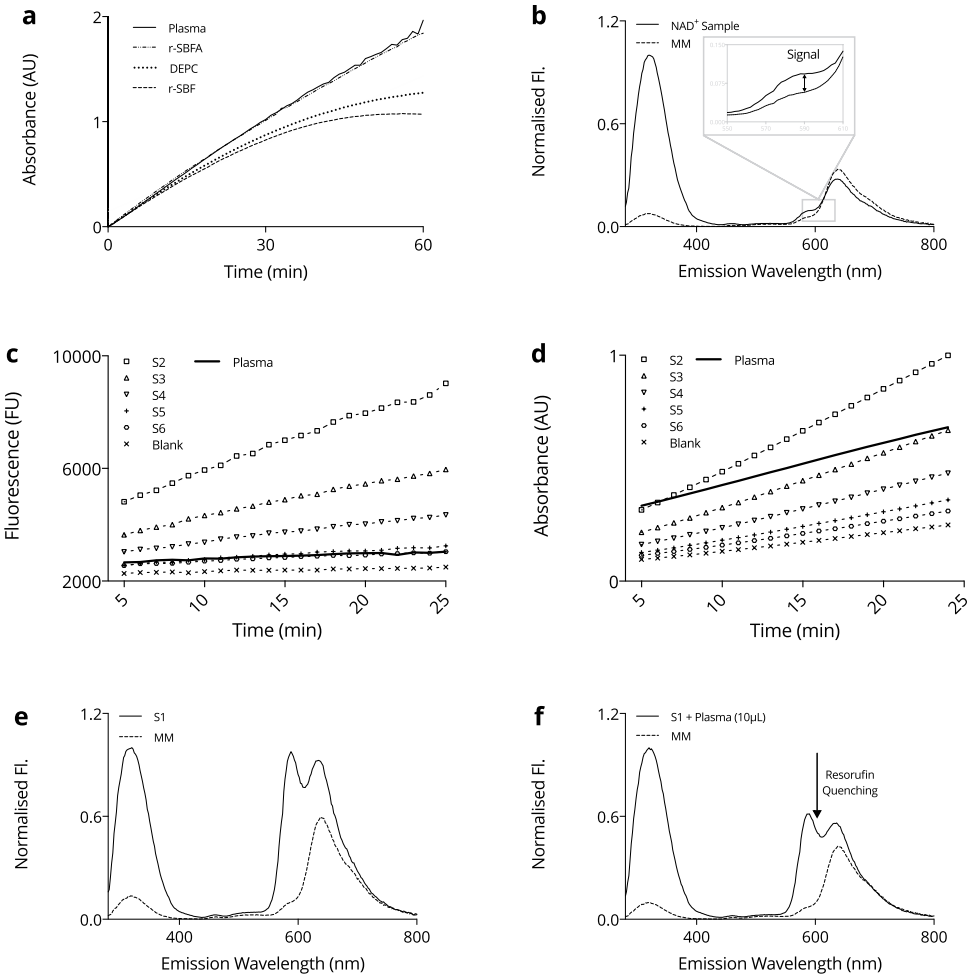

Figure 1. *Overview of the spectroscopic techniques*. (**a**) Comparison of the assay dynamics in different standard matrices utilising the absorbance unit (AU) readings obtained from DEPC water, revised simulated body fluid (r-SBF), revised simulated body fluid adjusted with albumin (r-SBFA) and human plasma, all spiked with 50 µL of 376.8 nM β-NAD standard (S2). (**b**) Fluorescence scan of the autofluorescence of the Master Mix (MM) and a NAD^+ sample as prepared in the actual assay reaction, scanned from $\lambda_{ex1} = 280\,nm - \lambda_{ex2} = 850\,nm$ in steps of $\Delta\lambda = 2\,nm$. The resorufin signal is indicated at $\lambda = 590\,nm$ in the detail view. (**c**) Enzyme dependent assay kinetics for β-NAD standards S1–S6 including a heparinised plasma sample and the blank of a given run using the fluorimetric method. (**d**) Enzyme dependent assay kinetics for β-NAD standards S1–S6 including a heparinised plasma sample and the blank of a given run using the colorimetric method. (**e**) Fluorescence scan of the autofluorescence of the Master Mix (MM) and β-NAD standard S1 as prepared in the actual assay reaction (S1 + r-SBFA + MM), scanned from $\lambda_{ex1} = 280\,nm - \lambda_{ex2} = 850\,nm$ in steps of $\Delta\lambda = 2\,nm$. (**f**) Visual representation of the resorufin quenching effect that occurs when a minuscule amount of heparinised plasma sample is added to the β-NAD standard S1.

tyrosine side chains fluoresces at this specific wavelength[26,27]. Moreover, human blood plasma is known to exhibit substantial autofluorescence around 500–600 nm due to physiologically occurring porphyrins[28–31].

In conclusion, we found the colorimetric method, displayed in Fig. 2, superior to the fluorimetric alternative concerning the measurement of $eNAD^+$ in human heparinised plasma.

Reaction time scale and $eNAD^+$ storage stability. To determine the time frame of the assay's linear operation, the absorbance readings for β-NAD standards S1 (753.6 nM) to S6 (23.5 nM) are depicted in Fig. 3a. Clearly, the relative reaction velocity, v_R, of S1 decreased, adopting a fluctuating and turbulent behaviour after about min 30, as seen in Fig. 3b,c, with the latter displaying the derivative of v_R, a_R. From this, we determined the time frame of linear operation between min 5–25 of reaction time.

The stability of $eNAD^+$ in human plasma remains an elusive and vague topic of investigation, suffering from a substantial lack of literature. However, $eNAD^+$ can be hydrolysed or degraded by multiple enzymes in

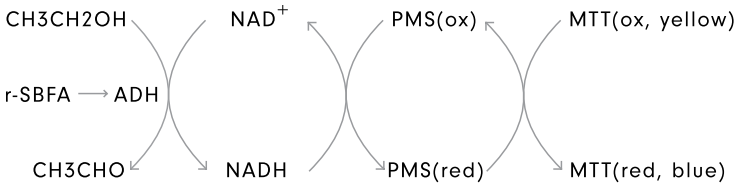

Figure 2. *NAD^+ cycling principle*. Schematic representation of the enzymatic alcohol dehydrogenae (ADH) cycling principle used to measure $eNAD^+$, involving phenazine methosulfate (PMS) as the primary and 3-(4,5-dimethylthiazol-2-yl)-2,5-diphenyltetrazolium bromide (MTT) as the secondary redox indicator dye. The method was inspired by the findings of Rhodes *et al.*[20] and adjusted with insights from the research of Zhu *et al.*[24] and O'Reilly *et al.*[13].

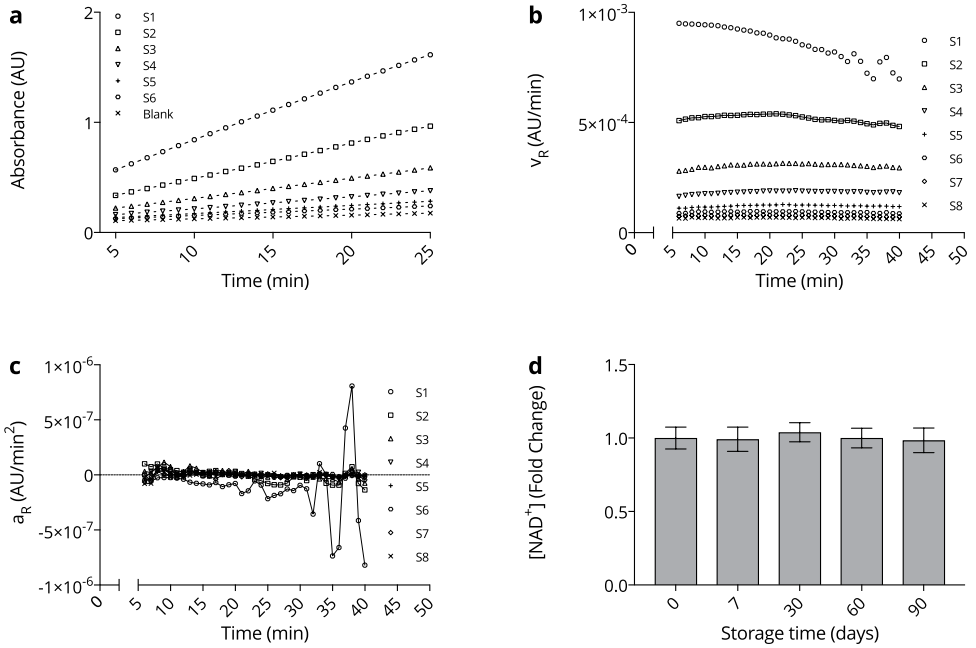

Figure 3. *NAD^+ assay and storage*. (**a**) Enzyme dependent assay kinetics for β-NAD standards S1–S6 and the blank of a given run during the assay validation: S1 (753.6 nM), S2 (376.8 nM), S3 (188.4 nM), S4 (94.2 nM), S5 (47.1 nM), S6 (23.5 nM), whilst standards S7 (11.8 nM) and S8 (5.6 nM) were omitted. (**b**) Relative reaction velocities (v_R) of standards S1–S8 during min 5–40 of the assay reaction. $n = 8$. (**c**) Relative reaction accelerations (a_R) of standards S1-S8 during min 5–40 of the assay reaction. $n = 8$. (**d**) Measured NAD^+ concentrations in human heparinised plasma stored at −80 °C for a given amount of time. No statistical significance was found when comparing the measured timepoints to the baseline ($d = 0$). $n = 6$. Statistics: Two-tailed, unpaired t-test with the confidence limits of $CL = 99\%$, as well as a two-way ANOVA (without repeated measures) adjusted with Tukey's multiple comparisons test featuring $CL = 99\%$. A significance level of $p < 0.01$ was applied to reject the null hypothesis. All error bars are given in terms of ±SD.

plasma, such as ADPribosyltransferases (ARTs), as well as NAD^+ - dependent glycohydrolases (NADases)[32,33]. Likewise, the knowledge of analyte storage stability remains crucial for investigational studies. Therefore, we tested $eNAD^+$ storage stability in human heparinised plasma samples at −80 °C over the course of three months, which is displayed in Fig. 3d. Indeed, no statistically significant difference was found between any of the measured time-points, at a significance level of $p < 0.01$, with the measured $eNAD^+$ concentration being (225.9 ± 16.7) nM. Hence, $eNAD^+$ can be considered stable in frozen human heparinised plasma for at least three months at −80 °C. These results were found to be in accordance with a murine study that demonstrated stability of $eNAD^+$ in frozen murine plasma for at least one week and the commercially available β-NAD, which was described to be stable for at least six months in aqueous solution[15,34].

Recapitulating, linear enzymatic behaviour was confirmed for min 5–25 of the assay reaction time and $eNAD^+$ was found to remain stable in frozen human heparinised plasma for at least three months.

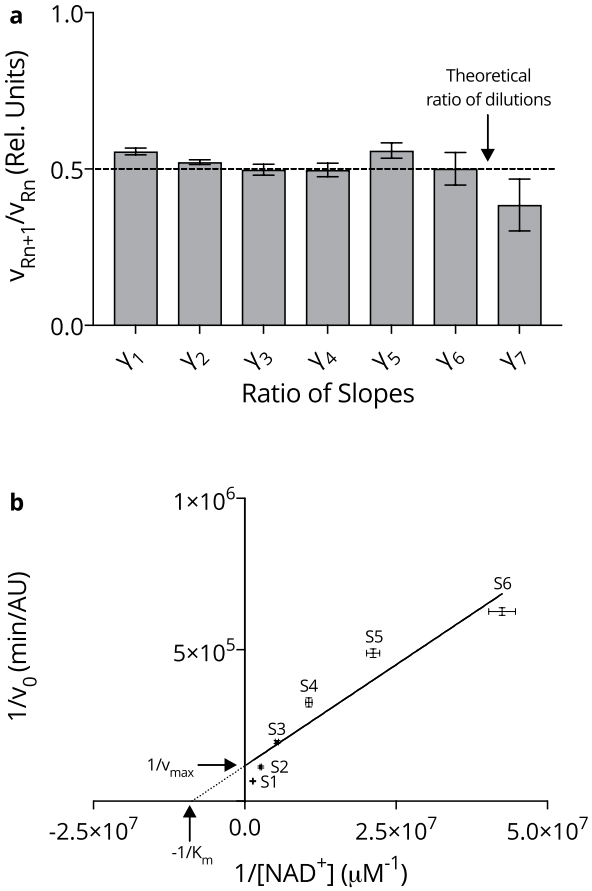

Figure 4. *NAD^+ assay linearity and enzyme kinetics.* (**a**) The ratio of the slope (v_R) of two sequential β-NAD standards, (n) and neighbour ($n+1$), is given by γ_n between min 5–25 of the assay reaction. $n=8$. (**b**) The Lineweaver-Burk Plot constructed for averaged, blank corrected, v_R data from eight Runs including S1–S6. $n=8$. Statistics: All error bars are given in terms of ±SD.

Standard linearity and enzyme kinetics. In order to accurately measure $eNAD^+$, it is a fundamental requirement that the v_R ratio of any two standards behaves identical to the ratio of their β-NAD concentrations. To examine this, the v_R ratio of standard, n, and neighbour $n+1$, was defined to be:

$$\gamma_n = v_{Rn+1}/v_{Rn} \quad (1)$$

The calculated results are presented in Fig. 4a. One can observe that γ remained relatively constant and closely resembled the 50% β-NAD standard dilutions for S1 (753.6 nM) to S7 (11.8 nM), with $\gamma_1 = 0.556 \pm 0.011$ to $\gamma_6 = 0.501 \pm 0.052$ and corresponding relative errors of δ_{γ_1}=1.96% and δ_{γ_6}=10.3%. However, there was an evident drop in the ratio when considering the change from S7 to S8 (5.9 nM), to $\gamma_7 = 0.385 \pm 0.083$, where the relative error increased to δ_{γ_7}=21.6%

Moreover, NAD^+ was employed as the new substrate in the double reciprocal Lineweaver-Burke plot[35]. The data displayed in Fig. 4b was constructed from eight independent assay reactions, where the Michaelis-Menten constant was found to be $K_m = (115 \pm 45.6)$ nM in addition to the maximum reaction velocity being $v_{max} = (8.58 \pm 3.13)\mu$mol min^{-1}.

In summary, the linear relationship between the standard slopes (γ) was confirmed for S1 (753.6 nM) down to S7 (11.8 nM), covering sufficiently the range of anticipated physiological concentrations of $eNAD^+$[13].

Reliability of NAD^+ detection in relation to albumin. Physiologically, serum albumin is the most abundant protein of human plasma. Patients with liver diseases can suffer from hypoalbuminaemia, presenting with levels below 35 g/L and drastic inter- as well as intrapatient variability, while healthy subjects typically feature levels in the range of 35–50 g/L. Hence, we studied the effect of varying albumin concentrations on the assay's predictive capability. As illustrated shortly, an ordinary regression line that runs not through the origin (nTTO, $v_R = mx + v_b$), as opposed to a regression line through the origin (TTO, $v_R' = mx + 0$), is subject to an inversely

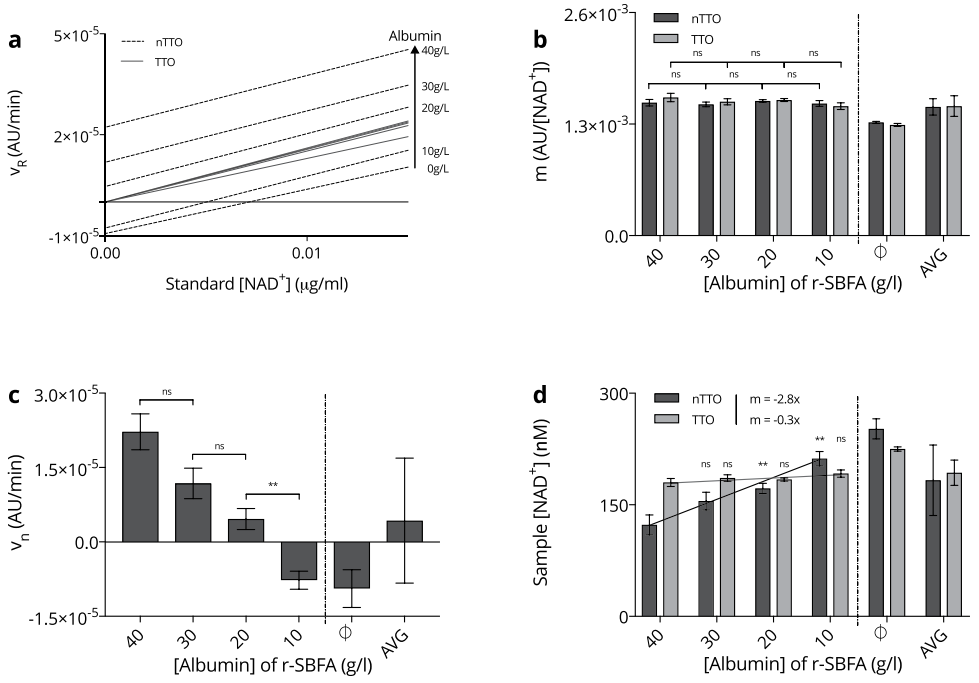

Figure 5. *Albumin dependency of the assay*. (**a**) Comparison of the calibration working curves not through the origin (nTTO, dotted) and to through the origin (TTO, solid) with respect to a varying albumin concentration in the β-NAD standards S1 (753.6 nM) through S6 (23.5 nM) of 0 g/L for the lowermost trace, 10 g/L, 20 g/L, 30 g/L and 40 g/L for the uppermost trace. $n = 3$. (**b**) Comparison of the slopes, m, of the calibration working curves obtained by linear regression analyses nTTO (dark) and to TTO (light) for different albumin concentrations. $n = 3$. (**c**) Variance of the y-axis intercept, v_n, of the regression lines nTTO with respect to varying albumin concentrations. $n = 3$. (**d**) Predicted pooled human heparinised sample eNAD$^+$ concentrations using calibration working curves constructed nTTO (dark) and to TTO (light) with respect to varying albumin concentrations. A regression fit over the physiological range of albumin concentrations yielded $y = -2.84\,x$nML/g + 236.5 nM ($R^2 = 0.9785$) for the nTTO and $y' = -0.34\,x$nML/g + 194 nM ($R^2 = 0.7706$) for the TTO approach. $n = 3$. Statistics: Two-tailed, unpaired t-test with the confidence limits of $CL = 99\%$, where a significance level of $p < 0.01$ was applied to reject the null hypothesis. $^{**}p < 0.01$. All error bars are given in terms of ±SD. The dotted line represents the physiological range of albumin concentrations.

proportional relationship between the albumin concentration of the matrix and the calculated eNAD$^+$ value, rendering it unworkable for analysis.

In order to demonstrate this, we evaluated various r-SBFA matrices featuring 0 g/L (r-SBF), 10 g/L, 20 g/L, 30 g/L and 40 g/L of albumin. In fact, one can observe from Fig. 5a, where nTTO and TTO calibration curves are contrasted, that their slopes remained relatively constant with varying concentrations of albumin for $m = (1.50 \pm 0.10)\,\text{ngAUmL}^{-1}\text{min}^{-1}$ and $m' = (1.51 \pm 0.12)\,\text{ngAUmL}^{-1}\text{min}^{-1}$, respectively. The individual values for the slopes of the nTTO and TTO approach are displayed more precisely in Fig. 5b. Here, no statistically significant differences between the neighbouring slopes of the physiological range of albumin concentrations (10–40 g/L) was found. However, Fig. 5a clearly demonstrates that an increase in the albumin concentration in the standard matrix caused an upward shift of the y-axis intercept, v_b, for lines constructed with a nTTO approach and is numerically presented in Fig. 5c, where the baseline can be seen to vary from $v_{b0} = (-9.40 \pm 3.81)\,\text{pgAUmL}^{-1}\text{min}^{-1}$ for no albumin (0 g/L) up to $v_{b40} = (4.31 \pm 12.6)\,\text{ngAUmL}^{-1}\text{min}^{-1}$ for 40 g/L of albumin, with an average value of $v_b = (4.31 \pm 12.6)\,\text{ngAUmL}^{-1}\text{min}^{-1}$, indicating a relative error of $\delta_{v_b} = 293\%$. No significant difference was found between v_{b40} and v_{b30} ($p = 0.0193$) as well as v_{b30} and v_{b20} ($p = 0.0289$), while v_{b20} and v_{b10} were, in fact, significantly different ($p = 0.0016$). Figure 5d reveals that the TTO method resulted in an average sample NAD$^+$ concentration of $x' = 193 \pm 17.0$ nM, indicating a relative error of $\delta_{x'} = 8.8\%$ in contrast to $x = 183 \pm 47.4$ nM for the nTTO approach, presenting with an escalated relative error of $\delta_x = 25.9\%$. Moreover, the TTO approach was fitted with an ordinary least squares regression, with CL = 99%, to produce $y' = -x0.34$ nML/g + 194 nM ($R^2 = 0.7706$), whilst the nTTO method featured $y = -x2.84$ nML/g + 237 nM ($R^2 = 0.9785$), representing an approximately 8 times higher dependence of estimated eNAD$^+$ on albumin. When measuring the estimated eNAD$^+$ amounts, the TTO method far outperformed the nTTO method. Merely a concentration of 30 g/L of albumin let to an insignificant increase of the estimated eNAD$^+$ ($p = 0.0361$), whilst 20 g/L ($p = 0.0049$) and 10 g/L ($p = 0.0007$) of albumin caused significantly different predicted eNAD$^+$ results. On the other hand, this effect was dampened when the TTO method was used as no significantly different estimated eNAD$^+$ concentrations were quantified at any of the given albumin concentrations, since $p < 0.01$.

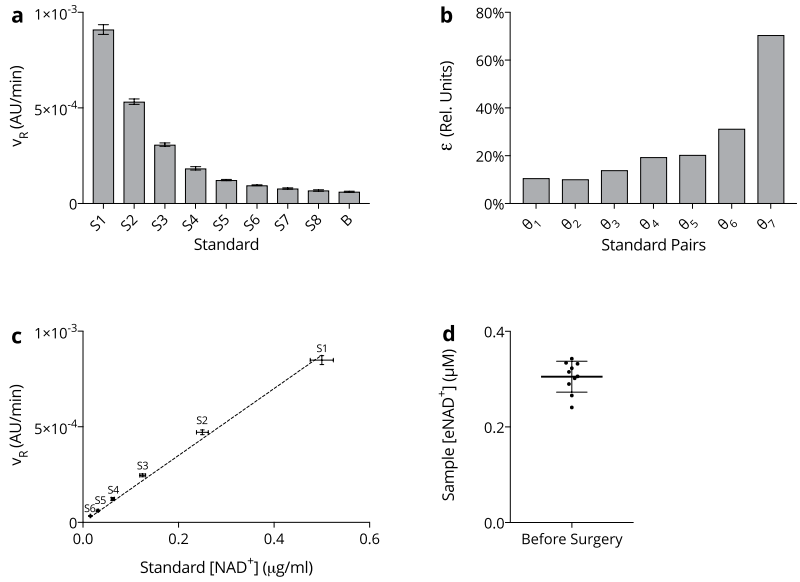

Figure 6. *NAD⁺ assay reproducibility*. (**a**) Mean relative reaction velocities (v_R) for β-NAD standards S1 (753.6 nM) through S8 (5.6 nM) and the blank measured between min 5–25 of the assay reaction. $n = 8$. (**b**) The ratio (ε_n) of standard deviations (σ_n), to the difference in relative reaction velocity (v_R) of two sequential β-NAD standards, (n) and neighbour ($n + 1$), represented by ψ_n. $n = 8$. (**c**) Calibration working curve constructed from the average slopes (v_R) of β-NAD standards S1 (753.6 nM) through S6 (23.5 nM), obtained from the eight-fold assay repetition. $n = 8$. (**d**) Blood samples were taken from patients scheduled to undergo hernioplasty and analysed for their eNAD⁺ concentration. Statistics: $n = 10$. Among the analysed, there were 8 male and 2 female patients, where the mean age averaged (52.1 ± 15.8) years, ranging from 29 to 75 years. The underlying diseases were inguinal hernia ($n = 7$), epigastric hernia ($n = 1$), hiatal hernia ($n = 1$) and umbilical hernia ($n = 1$). The overall average is displayed. Statistics: Two-way ANOVA (without repeated measures) adjusted with Tukey's multiple comparisons test with CL = 99%. A significance level of $p < 0.01$ was applied to reject the null hypothesis. ****$p < 0.0001$. All error bars are given in terms of ±SD.

Taken together, differing serum albumin levels cause inaccurate estimations of sample eNAD⁺ concentrations when the nTTO method is used. Strikingly, this effect was virtually eliminated, when calibration was constructed TTO, which lead to a substantially lower relative error as well as albumin related estimation bias.

Reproducibility, Sensitivity and Calibration. For the sake of evaluating the repeatability and robustness of the assay, the complete method was independently carried out eight times, with the respective slopes of the standard curves calculated within the interval of min 5–25 of the reaction time. The corresponding results are given in terms of the relative reaction velocity for each β-NAD standard n, v_{Rn}, and are displayed in Fig. 6a. In descending order the relative reaction velocities of standards S1 (753.6 nM) to S8 (5.9 nM) as well as the blanks were determined to be $v_{R1} = (9.10 \pm 0.28) \times 10^{-4}$ AU/min for S1 down to $v_{RS8} = (6.84 \pm 0.42) \times 10^{-5}$ AU/min for S8 and $v_{RB} = (6.18 \pm 0.33) \times 10^{-5}$ AU for the blank. The use of a two-way ANOVA (without repeated measures), adjusted with Tukey's multiple comparisons test, revealed that there was no significant difference observable between S6 (23.5 nM) and S7 (11.8 nM, $p = 0.012$), S7 and S8 (5.9 nM, $p = 0.373$), S7 and the blank ($p = 0.013$), or S8 and the blank ($p = 0.876$). In order to examine the potential implications for the precision of the assay when an additional β-NAD standard, $n-1$, was used for calibration, the ratio of the standard deviation, σ, to the difference in v_R, defines the introduced resolution error, ε:

$$\varepsilon_n = \frac{\sigma_n + \sigma_{n+1}}{v_{Rn} - v_{Rn+1}} \tag{2}$$

The respective values for ε are depicted in Fig. 6b, where the resolution error introduced by the consideration of S1 through S6 was found to be below $\varepsilon_{1-5} < 20\%$, whereas the inclusion of S7 (11.8 nM) and S8 (5.9 nM) lead to an escalated resolution error of $\varepsilon_6 = 30\%$ and $\varepsilon_7 = 70\%$, respectively. Having defined a threshold value of $\varepsilon = 20\%$, S7 and S8 were discarded from the assay for their lack of a statistically relevant v_R and inflation of ε.

Following this discovery, an ordinary least squares linear regression fit of the blank adjusted standard calibration curve was constructed from S1–S6 to run through the origin (TTO), shown in Fig. 6c, where $\rho = 0.9984$ and $R^2 = 0.9969$, with the corresponding slope $m = (1.75 \pm 0.04)\,\mathrm{ngAUmL^{-1}min^{-1}}$.

In order to present clinical findings of eNAD⁺ concentrations in blood plasma, we obtained heparinised blood samples from 10 fasting patients, who were scheduled to receive hernioplasty. Subsequent to obtaining the plasma samples, we determined the eNAD⁺ value to have a mean concentration of (305.2 ± 32.2) nM (range:

Reagent	Q (μmol)	Well (μL)	Plate (μL)
TEA	25.72	33.6	3528
EtOH	129	7.5	788
PMS	0.4	12.3	1292
MTT	0.1	41.4	4347
DEPC	—	41.1	4316
ADH	125 U	14.4	1512

Table 1. List of materials used for the preparation of 150 μL master mix per well, scaled to fit a standard 96 well plate (where 105 wells are considered necessary for the use of a pipetting basin). Note that the reagents employed are the products of this protocol so far, and have thus been preciously diluted and weighed into DEPC water.

240.9–342.7 nM). The graphical representation of this data is given in Fig. 6d. What is more, the analysis of one samples that was carried along all of the eight runs, resulted in a relative error of $\delta = 8\%$ in the measured $eNAD^+$ concentration.

When combining these results, the method was able to sense $eNAD^+$ in human heparinised plasma and in standards featuring concentrations of 753.6 nM (S1) down to 23.5 nM (S6) maintaining a striking calibration precision yet exhibiting a minor relative error.

Discussion

In this study, we established a reliable and robust colorimetric two-step enzymatic cycling assay to quantify $eNAD^+$ in human heparinised plasma, which can be used for high throughput screening of $eNAD^+$ levels in clinical discovery studies. The assay quantifies $eNAD^+$ by means of a two-step enzymatic cycling reaction, based on ADH (Fig. 2). An albumin modified r-SBF was used to warrant physiological enzymatic activity. In addition, we evaluated assay linearity, reproducibility and confirmed long-term storage stability of $eNAD^+$ in frozen human heparinised plasma.

However, the correct blood collection method is of the essence. We employed lithium heparin tubes during the acquisition of blood samples as the common chelating agent K3EDTA is in fact a potent inhibitor of ADH, and would therefore eradicate linear enzyme behaviour[36]. In order to secure optimal enzyme activity, the concentrations of ADH as well as its substrate, ethanol, were chosen to be well beyond their point of saturation, so that any effect of even an ever so slight variation in their respective amounts would be essentially nullified[24].

In order to validly calculate $eNAD^+$ levels in human plasma, it was imperative to employ an appropriate and *in vivo*-like standard matrix. Physiologically speaking, albumin is the most abundant plasma protein, with a concentration in the range of 35–50 g/L, whilst being the main carrier of zinc in blood, as approximately 80% of all plasma zinc is bound to albumin[37]. Thus it serves as a major zinc donor in blood, comprising part of the so called exchangeable pool, which, given zinc's role as a blood trace element, is crucial to the proper functioning of ADH. In fact, a catalytic zinc ion binds to ADH's Cys-43, Cys-153 and His-66 amino acid residues, which was the primary rationalisation for our addition of albumin into r-SBF, since zinc is neither present in r-SBF, nor in DEPC[38]. This could very well explain the evident deviation from linearity after about 30 min in all zinc-free matrices, indicating a decreased ADH reaction speed and successive plateauing substrate conversion rate. However this was alleviated through the addition of 40 g/L of albumin to r-SBF, as demonstrated in Fig. 1. Indeed, we hypothesise that, under the assumption that albumin's affinity for zinc is not infinitely large, some of these zinc ions will be competed for, and eventually be seized by ADH. In addition, the extreme pH milieus, combined with the heat incubation upon pyridine extraction, will cause a release of zinc from albumin, facilitated by its denaturation. Results obtained from the comparison of different standard matrices, presented in Fig. 1a, seem to corroborate this hypothesis, for r-SBFA replicated the assay kinetics observed in human heparin plasma almost indiscriminately.

Moving on to the analyte isolation, a heat based dichotomous pH extraction procedure was utilised to extract and amass purified versions of either NAD^+ at pH 1.5 or NADH at pH 12.5, as can be seen in Table 5, in consideration of Lowry *et al.* and Lilius *et al.*[18,25]. An illustration of this process is given in Supplementary Fig. S.2. As the assaying method was intended to quantify $eNAD^+$ plasma levels in exploratory studies, it was necessary to test storage stability of $eNAD^+$ in human heparinised plasma at −80 °C. This was done to evaluate the possibility, that $eNAD^+$ would be hydrolysed by ectoenzymes from the family of NADases such as CD38 or ADPribosyltransferases like ART2[5,39]. Subsequently, we confirmed the stability of $eNAD^+$ in frozen human plasma for at least three months, which was in accordance with a murine study that demonstrated its stability for at least one week, as well as the known stability of β-NAD in aqueous solution for at least six months[15,34].

With respect to the fluorimetric evaluation as an alternative quantification method, the reader is pointed to some potentially detrimental properties of human blood plasma that hinder the measurement of $eNAD^+$ using resazurin. First and foremost, naturally occurring porphyrins cause the autofluorescence of human blood plasma to exhibit two prominent spikes at 630 nm and 590 nm, of which the latter one happens to be at the exact frequency resorufin fluoresces at[28]. It is further known that these autofluorescence spectra can vary substantially over the range of 500–600 nm, due to immense variations in plasma porphyrin levels, which are common in patients with cancer[29–31]. What is more, another biological molecule with a broad autofluorescence band around 500–600 nm is bilirubin[40]. The vast fluctuations in bilirubin levels, especially in patients suffering from liver disease can therefore cause significant baseline shifts that are very difficult to correct for. Having used resazurin instead

Standard	β-NAD (n*M*)	β-NAD (ng/mL)
S1	753.6	50.00
S2	376.8	25.00
S3	188.4	12.50
S4	94.2	6.25
5	47.1	3.13
6	23.5	1.56

Table 2. List of β-NAD standards prepared in DEPC water with respective concentrations.

of MTT, we immediately realised the almost complete eradication of the signal in plasma, whilst the standards remained readily quantifiable. Moreover, we tested the impact of adding a small amount of a plasma sample to the first β-NAD standard, S1, upon which its obtained signal experienced a sharp drop, clearly demonstrated in Fig. 1e,f. Besides the aforementioned reasons, a few possible explanations are herein presented that could be responsible for this apparent quenching of the resorufin signal at the 590 nm emission band. In fact, Montejano *et al.*[41] described that resorufin is quenched by quinones at this very frequency band[41]. Given the endogenous nature of these molecules, the sharp drop in resorufin's fluorescence upon the addition of a small plasma quantity (which even contained physiological eNAD$^+$ concentration) supports this hypothesis and explains why eNAD$^+$ is not measurable in a full plasma sample via fluorescence spectroscopy.

In comparison to other measuring procedures of NAD$^+$, it has to be stated that eNAD$^+$ has been studied in a far lesser extent than iNAD$^+$, most likely for its drastically reduced concentration, from 10–40 M intracellularly to 240–290 nM extracellularly, which presents nontrivial analytical challenges[11–13]. Alternative to the quantification of chromogenic or fluorescent signals, the concentration of iNAD$^+$ has been measured using a multitude of sophisticated high-performance liquid chromatography (HPLC) methods such as HPLC-UV[42,43], as well as HPCL-NMR[44,45], whilst, in a more specialised scenario, HPLC-UV[11,46] and HPLC-MS[47,48], have been employed to evaluate murine erythrocyte intracellular NAD$^+$ (iNAD$^+$) levels. These methods have been used predominantly to measure iNAD$^+$, while only very few could be used to study eNAD$^+$ directly without any preceding concentrating steps, for their relatively high limit of quantification. However, Liang *et al.*[15] used a modified version of the HPLC-MS, namely the electrospray ionisation HPLC-ESI-MS to successfully measure eNAD$^+$ in murine blood[15]. Nonetheless, for all analytical methods involving calibration methods, the standard matrix has to exhibit comparable traits to the authentic biological sample matrix and should either be a laboratory prepared or analyte-stripped version of the matrix of interest. In fact, Liang *et al.*[15] used HPLC grade water in their HPLC-ESI-MS analysis, which seemed to be common practice amongst other HPLC based analyses[15]. This opens up the analysis of NAD$^+$ to be subject to significant signal distortions through imperfect enzyme kinetics, signal masking by other analytes or by means of ionisation suppression[14]. In addition, the apparatus required for HPLC analyses tends to be rather expensive, therefore limiting their availability to the general scientific community, whereas our enzymatic cycling method merely required an ordinary microplate reader, present in virtually all laboratories by default, in addition to any kind of transparent 96 well plate.

When it comes to plasma compounds that could affect the assays performance, we postulate that ADH is the main source of measurement variation, as it represents the main rate limiting factor in the redox dye conversion reaction. For instance, human isoforms of ADH are generally inhibited by common drugs such as aspirin or H2 receptor blockers in the form of cimetidine or ranitidine[49,50]. These drugs might be present in the plasma of individual patients at distinct concentrations. What is more, these drugs might very well resist, in part, the extraction, neutralisation and deproteinisation steps, thereby modulating the activity of ADH in the assay reaction. This could cause eNAD$^+$ measurement variations at an inter- as well as intrapatient levels. ADH is characterised further through a modulatory effect by different hormones, such as growth hormones, epinephrine or estrogens which act in a stimulatory manner, while thyroid hormones[51] and androgens can inhibit ADH's activity[52,53]. Therefore, varying baseline levels of these hormones upon blood collection could further impact the behaviour of ADH in the plasma sample. However, this assumption seems to be more theoretical as the extraction step (60 heat incubation for 10 min at pH 1.5) is expected to denature virtually all proteins and hormones. It is well known that ADH features broad specificity to aliphatic alcohols other than ethanol. For instance, it oxidises methanol to produce formaldehyde. In fact, methanol is of varying concentration in human blood, partly due to dietary preferences for artificial sweeteners such as aspartame[54]. Fasting blood levels of methanol were found to be on average 168 μmol/L, which converts to 5.39 mg/dL[55]. However, the assay procedure will cause a 6-fold dilution of methanol levels, yielding an approximate concentration 1 mg/dL, which is less than 1% of the ethanol concentration in the MM (being 125 mg/dL). Furthermore, ADH can also metabolise retinol (Vitamin A), which is present in blood plasma at levels around 60 μg/dL[56]. It is due to the fact that ethanol's concentration, as key substrate of ADH in the MM, was chosen to lie well beyond the point of saturation, that neither methanol nor retinol are expected to have a prominent effect on the measured eNAD$^+$, for their minuscule concentrations. In summary, we hypothesise that hormones, proteins and vitamins endogenous to human blood, will produce merely negligible effects on the assay, thanks to the selection of our extraction and neutralisation procedure, which provides an immensely harsh environment that most of these compounds cannot withstand.

The presented method was exhaustively tested in human heparinised plasma and the analysis as well as the experimental protocol, attached to this article as Supplementary Method S.1, account for immense variations in the standard and sample matrices, due to albumin fluctuations. In respect of the findings displayed in Fig. 5, it was evident that a regression line TTO would be used for all measurements, as it first and foremost increased

Reagent	Supplier	Amount (g)
NaCl	SIGMA, USA, Catalog No: DE71376	5.403
$NaHCO_3$	SIGMA, USA, Catalog No: DES5761	0.740
Na_2CO_3	SIGMA, USA, Catalog No: DES7795	2.046
KCl	ROTH, GER, Catalog No: 6781.1	0.225
KH_2PO_4	ROTH, GER, Catalog No: 3904.1	0.138
$MgCl_2{\cdot}6H_2O$	ROTH, GER, Catalog No: HN03.1	0.311
HEPES	ROTH, GER, Catalog No: 9105.4	11.928
$CaCl_2{\cdot}2H_2O$	ROTH, GER, Catalog No: HN04.1	0.388
Na_2SO_4	SIGMA, USA, Catalog No: S6547	0.072
BSA	SERVA, GER, Catalog No: 47330.03	40

Table 3. List of materials used for the preparation of 1000 mL of a revised simulated body fluid adjusted with albumin (r-SBFA) where the pH was adjusted to be 7.5, using approximately 0.8 mL 1.0 N NaOH. The composition of the r-SBF without albumin was adopted from Oyane *et al.*[63].

Formulation	Na^+	K^+	Mg^{2+}	Ca^+	Cl^-	HCO_3^-	HPO_4^-	SO_4^-	Buffer
Blood Plasma	142.0	5.0	1.5	2.5	103.0	27.0	1.0	0.5	—
Original SBF	142.0	5.0	1.5	2.5	148.8	4.2	1.0	0.0	Tris
Corrected (c-SBF)	142.0	5.0	1.5	2.5	147.8	4.2	1.0	0.5	Tris
Revised (r-SBF)	142.0	5.0	1.5	2.5	103.0	27.0	1.0	0.5	HEPES
Modified (m-SBF)	142.0	5.0	1.5	2.5	103.0	10.0	1.0	0.5	HEPES

Table 4. Common simulated body fluids compared to human blood plasma, where ionic concentrations are given in mM. The table was extracted from the findings of Oyane *et al.*[63].

the robustness of the method and secondly it was simply not feasible to produce a tailored albumin blank for every human heparinised plasma sample due to practical reasons. Moreover, albumin concentrations are rarely known, as they are not covered by standard blood chemistry tests. This, is as the evidence gathered and presented in Fig. 5a,c, illustrates the high dependency of the y-axis intercept, v_b, of the assay's nTTO calibration curve on the albumin concentration of the standard matrix. Hence, when utilising those calibration curves to estimate the $eNAD^+$ of an actual plasma sample, one will obtain very uncertain and unreliable results, as v_b in the equation of the regression line, when extrapolating for an unknown amount, x, takes the role as a subtractor of v_R, and, given that we are dealing with relatively small values of m in the denominator, causes escalated fluctuations of the resulting value. On a critical note, an estimation of the random error that arise when preparing the standards and the total random error, including the final addition of the MM to the standard, are given below. For this purpose, the common propagation of uncertainty analysis was conducted, where pipetting as well as applicable preparation errors, such as weighing scale or glassware uncertainties, were considered. For any given measurement of the experimental factors a, b and c resulting variable, Q, that is the combination of sums and differences, $a + b$, $Q = a + b - c$, the uncertainties, Δ, add in quadrature, that is;

$$\Delta Q = \sqrt{(\Delta a)^2 + (\Delta b)^2 + (\Delta c)^2} \tag{3}$$

On the other hand, if R, is the resulting variable of a multiplication or division, $R = \frac{a+b}{c}$, then the fractional uncertainties add in quadrature;

$$\frac{\Delta Q}{Q} = \sqrt{\left(\frac{\Delta a}{a}\right)^2 + \left(\frac{\Delta b}{b}\right)^2 + \left(\frac{\Delta c}{c}\right)^2} \tag{4}$$

In fact, this resulted in the estimation of the random relative error in preparing S1 of $\delta_{S1} = 4.84\%$, increasing to $\delta_{S6} = 5.20\%$ for S6, while the total relative error after the addition of the MM for S1 was determined to be $\delta_{T1} = 8.29\%$, increasing to $\delta_{T6} = 8.50\%$ for S6. Obviously, this error can be minimised by preparing reagents in aliquots, where possible.

On a practical note, experimenter is able to perform the whole method given in Supplementary Method S.1, in approximately 90 min. When employing a commonly used 96 well plate this would imply a total experiment time of roughly 1 min per sample, representative of a substantial increase in time efficiency when compared to the commonly employed HPLC quantification methods, that usually require 10–60 min of reaction time per sample analysed.

At a molecular level, $eNAD^+$, has been identified to be of intricate involvement in a substantial number of regulatory pathways as a coenzyme for ADPribosyltransferases (ARTs), NAD^+-dependent protein deacetylases of the Sir2 family (SIRTs) as well as NAD^+-dependent glycohydrolases (NADases), in addition to serving as a precursor of the calcium mobilising molecule cADPR (cyclic ADP-ribose)[32,33,57]. The highly modulating properties

Extraction Buffer added (mL)	NAD^+ extraction (pH)	NADH extraction (pH)
0 mL (plasma pH)	7.84 ± 0.05	7.89 ± 0.03
1 mL	4.96 ± 0.06	10.29 ± 0.19
2 mL	3.87 ± 0.05	11.48 ± 0.05
3 mL	2.10 ± 0.03	12.22 ± 0.03
4 mL	1.47 ± 0.02	12.58 ± 0.05
5 mL	1.24 ± 0.01	12.67 ± 0.02
6 mL	1.11 ± 0.01	12.81 ± 0.02

Table 5. Dichotomous pH extraction procedure to extract purified versions of either of the pyridine nucleotides, that is, NAD^+ or NADH in consideration of Lowry *et al.*[62] and Lilius *et al.*[25] in three fold repetition.

of $eNAD^+$ are, on this note, underscored by its substantial involvement in highly specific and selective ectoenzymes, namely NADases such as CD38, ADPribosyltransferases like ART2 or its key role in purinergic signalling through P2X7 or P2Y[5,39,58]. Leading on to the systemic involvement of $eNAD^+$ in immunological processes and its relevance to human physiology, the plasma membrane of eukaryotic cells was long believed to be impermeable to NAD^+. Yet, after some initial findings of passive pyridine nucleotide transmembrane-transport, Bruzzone *et al.*[59], successfully identified this elusive NAD^+ transporter as the hexametric hemichannel Cx43[59]. Cx43 is a ubiquitous transmembrane protein, that, when juxtaposed on adjacent cells, forms local high density areas at the gap junctions between these cells[60].

In conclusion, we herein present a robust method for the measurement of $eNAD^+$ in human heparinised plasma standardised, validated and optimised for low-cost high throughput screening applications using off-the-shelf materials, including standard laboratory equipment such as microplate readers. This method was established to help validate the future resumption of our working hypothesis being that $eNAD^+$ is involved in extracellular paracrine signalling with implications for various systemic diseases. Moreover, our method facilitates the translational research of $eNAD^+$ and its role in aging as well as the pathogenesis of oncologic or other systemic diseases by lowering the economic barriers of expensive experimental devices.

Methods

Establishment of the cycling method. The protein alcohol dehydrogenase (ADH, EC1.1.1.1) from Saccharomyces cerevisiae was employed to measure the pyridine nucleotides NAD^+ and NADH, due to its specificity for NAD^+ as a coenzyme, which, given the cycling nature of the application promotes NADH to the status of being a coenzyme as well[61]. Illustratively, a schematic of the principle behind this cycling assay is provided in Fig. 2, where the reader can follow the path of the electrons which are transferred during one cycle of the assay. Initially, the NAD^+ dependent dehydrogenase ADH catalyses the conversion of ethanol into acetaldehyde (ethanal)[20], reducing its coenzyme NAD^+ to NADH in the process. In turn, this reduced pyridine nucleotide donates an electron to the secondary redox indicator dye, 3-(4,5-dimethylthiazol-2-yl)-2,5-diphenyltetrazolium bromide (MTT), via a preceding coupled reaction with the primary indicator dye, phenazine methosulfate (PMS). The reduction of MTT, and subsequent formation of formazan, can then be assayed colorimetrically and linked to the concentration of NAD^+ (and NADH).

In order to distinguish NAD^+ from NADH, the impeccable works of Lowry *et al.*[62] on 'The Stability of Pyridine Nucleotides', provided us with a method of extracting the respective nucleotides by means of heat-incubating them in different pH milieus. Thereby, NAD^+ could be extracted through the addition of a strong acid, destroying all NADH molecules, whereas NADH is extracted with a strong base, destroying all NAD^+ molecules. The extraction steps were chosen to feature pH 1.5 for the NAD^+ extraction and pH 12.5 for the NADH extraction. In order to enzymatically measure the respective pyridine nucleotides, the samples were neutralised at pH 7.4 in order to shift the pH into the physiological working range of ADH. The role of r-SBFA in this method was to emulate heparinised blood plasma as the standard matrix.

Preparation of chemicals. The assay reaction was initialised, and thus the signal was induced through a Master Mix (MM), which, apart from NAD^+, contained all the molecules required for the cycling reaction which consisted of the following reagents: Alcohol Dehydrogenase from yeast in suspension, EC1.1.1.1 (ADH, SIGMA, USA, Catalogue No: 10127558001), thiazolyl blue tetrazolium bromide (MTT, Sigma, USA, Catalogue No: M2128), phenazine methosulfate (PMS, Sigma, USA, Catalogue No: P9625), ethanol (100%), Triethanolamine (TEA, Sigma, USA, Catalogue No: 90279), and diethyl dicarbonate (DEPC, Sigma, USA, Catalogue No: D5758) water. As employed in the MM, the TEA Buffer, as well as the ADH solution were prepared in a ten-fold dilution with DEPC water, whilst PMS was prepared as a 10 mg/mL solution and MTT as a 1 mg/mL solution in DEPC water. In Table 1, a list of materials is given, featuring the molar make-up of the MM and the respective quantities of the molecules employed for a single well (150 µl of MM) and extended to an entire plate (extended to 105 wells, to facilitate the use of a pipetting basin). Upon the evaluation of a fluorimetric method, MTT was substituted with resazurin (Sigma, USA, Catalogue No: R7017).

The NAD^+ and NADH extraction and neutralisation buffers were then prepared in DEPC water, where the NAD^+ extraction buffer consisted of a 0.3 N HCl solution and the neutralisation buffer comprised equal parts of 0.36*N* TEA-HCl (ACROS, USA, Catalogue No: 170051000) and 0.6*N* KOH. Analogously, 0.3N KOH was used for the NADH extraction buffer, whilst the neutralisation buffer was composed of 23% 0.36N TEA-HCl, 23% 0.6N

HCl and 54% DEPC water. PMS and MTT stock solutions were stored in aliquots at −20 °C until use. The MM was prepared freshly just prior to measurement to prevent auto-oxidation of PMS and MTT as well as a denaturation of ADH.

Preparation of stock solutions. The linearity, sensitivity, and specificity of the assay was determined with β-NAD (Sigma, USA, Catalogue No: N6522) as a reaction standard used for the construction of calibration curves. Firstly, a 1 mg/L stock solution of β-NAD in DEPC water was prepared, followed by a thousand-fold dilution in DEPC water. Successively the first calibration standard (S1), was obtained to entail a concentration of 0.5 μg/mL (753.6 nM) by a further one to one dilution of 500 μL in 500 μL DEPC. Afterwards, 5 additional serial dilutions constituting 500 μL of previous Standard in 500 μL DEPC water were performed to obtain S2 (376.8 nM) through S6 (23.5 nM), respectively, forming a total of six calibration standards, which are summarised in Table 2. Initially, two further dilutions were prepared as S7 with a concentration of 11.8nM and S8 with a concentration of 5.9 nM, however these were excluded from the assay upon evaluation of their suitability as calibration standards. Until use, prepared β-NAD aliquots were stored at −80 °C.

Standard matrix preparation. When operating enzymatic assays, and subsequent sample concentration extrapolation using calibration curves, it is essential to carry the standards (S1–S6) in a matrix that adequately reflects and resembles the physiological properties of human blood plasma, the *in vivo* matrix of $eNAD^+$. Note that, deriving a plasma based standard matrix completely free of NAD^+ is not feasible because of the endogenous nature of this analyte. For this reason, several commonly used simulated body fluids (SBF) were theoretically compared to blood plasma based on their ionic composition and buffering capabilities, and are displayed in Table 4[63]. Due to its remarkable ionic resemblance to blood plasma, we employed a revised simulated body fluid (r-SBF) to serve as the standard matrix. In addition to that, r-SBF contained HEPES buffer, which features an acid dissociation constant of $p_{ka} = 7.5$, thus more closely resembling the buffering nature of plasma than the otherwise commonly used Tris buffer, exhibiting $p_{ka} = 8.07$. Although the process for finding this standard matrix is presented and discussed in the following sections, it was found that the addition of albumin has proven crucial in emulating the assay's enzyme kinetics in human plasma. Finally, a list of materials used to prepare 1000 ml of a revised simulated body fluid adjusted with albumin (r-SBFA) in DEPC water is given in Table 3, below. In fact, the albumin concentrations of the r-SBFA were evaluated with respect to their impact upon the assay performance at 0 g/L (r-SBF), 10 g/L, 20 g/L, 30 g/L and 40 g/L. The prepared r-SBFA was stored in aliquots at −20 °C, until use.

Blood sample collection. Human peripheral venous blood from surgical patients, approved by the Charité ethics committee (Ethikkommission der Charité Universitätsmedizin Berlin, EA1/291/17 and EA1/018/17), was collected - after having obtained informed consent - into lithium heparin, complying with local regulatory guidelines and the Declaration of Helsinki. Samples were promptly centrifuged at 2500 g for 15 min at 4 °C in order to separate the plasma from all corpuscular parts of the blood, which was successively collected and snap frozen in liquid nitrogen. The resulting plasma aliquots were then transferred to a −80 °C freezer, where they were stored until being assayed for $eNAD^+$ concentrations. In addition to our own storage time evaluation, literature provided sufficient evidence that $eNAD^+$ in frozen plasma, as well as the commercially available β-NAD, used in this method, were stable under these conditions[15,34].

NAD extraction protocol. As previously described, we based the extraction procedure of NAD^+ and NADH on the findings of Lowry *et al.*[18], adjusted with insights from Lilius *et al.*[25] and O'Reilly *et al.*[13]. Heparin plasma samples were treated with 0.3N HCl to extract NAD^+ and 0.3N KOH to extract NADH, following their collection from the −80 °C freezer and after subsequent thawing at room temperature. This is since NAD^+ is known to be stable for at least half an hour at room temperature[15]. Initially, 300 μL of sample were transferred into a new tube for NAD extraction and 30 μL sample + 270 μL r-SBFA for NADH extraction. Upon addition of the acid and base solutions for pyridine nucleotide extraction, the samples were vortexed and then incubated at 60 °C for 10 min. Following this, the samples were promptly equilibrated on ice for 10 min. Subsequently, the samples were neutralised so as they would exhibit ADH's optimum working pH of 7.4 through the addition of 300 μL of their respective neutralisation buffers. The resulting pH values after extraction were confirmed with a standard glass pH probe and the data is presented in Table 5. For illustrative purposes, a flowchart of this process is depicted in the Supplementary Fig. S.2.

Pipetting and plate reader settings. Before beginning the assaying phase of the method, the MM was prepared on ice without MTT, PMS or ADH, in order to prevent auto-oxidation of PMS or MTT and denaturation of ADH. Prior to pipetting the samples into the plate, the neutralised samples were centrifuged at 16.000 g for 10 min at 4 °C and the supernatant was successively pipetted into the wells. Standard dilutions (S1 to S6) were supplemented with 50 μL of r-SBFA that had been extracted and neutralised in the same manner as the samples, to provide the standard matrix similar to human plasma. Analogously, 50 μL of DEPC water was added to the samples to be measured in order to simulate the DEPC used in the β-NAD standard dilutions. Subsequently, ADH, MTT and PMS were added to the MM, 150 μL of which was pipetted into every well, resuspending twice. Afterwards the plate was stored at room temperature in the dark for 5 min prior to assaying. The absorbance of the samples was then measured at 565 nm in the microplate reader Infinite® 200 PRO (Tecan, Switzerland) in a temperature of 25 °C to prevent significant build-up of bubbles, which occurred at 37 °C. Moreover, the Infinite 200 PRO further served to assess fluorescence at 590 nm and perform autofluorescence scans. All measurements were conducted in duplicates and averaged.

Enzyme kinetics. Since NAD^+ is the coenzyme in the specific reaction between ADH and ethanol, one can consider the concentration of NAD^+ to be rate limiting as the ethanol concentration was chosen well beyond the point of saturation in the MM. NAD^+ can therefore be regarded as the new substrate and, consequentially, be used in a graphical method to obtain the Michaelis Menten constant, K_m, and the maximum reaction velocity, v_{max}, from the double reciprocal Lineweaver-Burke plot described in Lineweaver *et al.*[35]. Here, the y-axis is given by v^{-1}, and v_0 represents the initial reaction velocity and the x-axis is represented by $[NAD^+]^{-1}$, the reciprocal of the analyte concentration. The double reciprocal Lineweaver-Burk plot facilitated the graphical evaluation of the Michaelis Menten constant, K_m, given by the negative reciprocal of the x-axis intercept, in addition to the maximum reaction velocity, v_{max}, given by the reciprocal of the y-axis intercept.

Regression analysis. As illustrated shortly, the use of an ordinary regression line not through the origin (nTTO, $v_R = mx + v_b$), as opposed to a regression line through the origin (TTO, $v_R = mx + 0$), was subject to an increased baseline noise and higher $eNAD^+$ estimation bias, introduced by the varying albumin concentrations in the standard matrix. Thus, the TTO method allowed for an albumin independent quantification of $eNAD^+$. The relative reaction velocity, v_R, is made up of the y-axis intersection,v_b, and the slope of the absorbance curve, m.

Reliability, reproducibility and linearity. For the sake of evaluating the repeatability and robustness of the assay, a quantification of $eNAD^+$ in healthy human heparinised plasma was conducted with eight independent measurements, featuring the thorough and individual conductance of the complete and previously described experimental protocol, including eight independent standard dilutions, as well as eight individually collected human heparinised plasma samples from a singular subject. Subsequently, these data were utilised to obtain the interval were the enzyme kinetics of the assay reaction occurred in a linear fashion, as well as to confirm the linear relationship between the standard β-NAD^+ sequential dilutions and their respective relative reaction velocities.

NAD^+ storage stability. Being of considerable controversy, the stability of $eNAD^+$ in frozen plasma suffers from a definitive lack of data in the literature. However, upon the conductance of studies involving human samples, such knowledge is not only of paramount ethical importance but also crucial for the validity of designed experiments, in particular for the algorithm used to store such samples. Therefore healthy human heparinised plasma samples were prepared and stored at −80 °C as described above, before being assayed for $eNAD^+$. The baseline measurement consisted of an immediate thawing and assaying of the first sample, whilst additional measurements were performed up to three months.

Evaluation of a fluorimetric alternative. In consideration of Rhodes *et al.*[20], we explored the ability of a fluorimetric method to sense $eNAD^+$ in human heparinised plasma[20]. For this purpose, we replaced MTT in the MM of the colorimetric method with resazurin, which, upon being reduced, forms the highly red fluorescing resorufin. Moreover, we paid close attention to conserve the number of moles of resazurin compared to MTT participating in the reaction as well as the volume of all suspensions that are part of the MM.

Statistics. Statistical analysis was conducted in Graphpad's Prism 7 (GraphPad Software, La Jolla, CA, USA). Concerning the evaluation of the $eNAD^+$ storage stability, the data were analysed using a two-tailed, paired t-test with confidence limits of CL = 99%, as well as a two-way ANOVA (without repeated measures) adjusted with Tukey's multiple comparisons test featuring CL = 99%. The statistical evaluation of the assay's dependence upon the albumin concentration of the standard matrix was conducted using a two-tailed, unpaired t-test with the confidence limits of CL = 99%. With regards to the reproducibility of the aforementioned method, significance was assessed between two neighbouring standard signals using two different methods, namely a simple, two-tailed, unpaired t-test with the confidence limits of CL = 99%, as well as using the more stringent conditions of a two-way ANOVA (without repeated measures) adjusted with Tukey's multiple comparisons test with CL = 99%. Regression analysis of the calibration working curve was performed with the gold standard of an ordinary least squares fit, yielding a Pearson Correlation Coefficient, ρ, as well as a coefficient of determination, R^2, with CL = 99%. Overall, an alpha value of $p < 0.01$ was applied.

References

1. Massudi, H. *et al.* Age–associated changes in oxidative stress and NAD+ metabolism in human tissue. *PLoS ONE* **7**, e42357, https://doi.org/10.1371/journal.pone.0042357 (2012).
2. Massudi, H., Grant, R., Guillemin, G. J. & Braidy, N. NAD+ metabolism and oxidative stress: the golden nucleotide on a crown of thorns. *Redox Report* **17**, 28–46, https://doi.org/10.1179/1351000212Y.0000000001 (2012).
3. Partida-Sanchez, S. *et al.* Chemotaxis of Mouse Bone Marrow Neutrophils and Dendritic Cells Is Controlled by ADP–Ribose, the Major Product Generated by the CD38 Enzyme Reaction. *The Journal of Immunology* **179**, 7827–7839 (2007).
4. Haag, F. *et al.* Extracellular NAD and ATP: Partners in immune cell modulation. *Purinergic Signalling* **3**, 71, https://doi.org/10.1007/s11302-006-9038-7 (2007).
5. Lazarowski, E. R., Boucher, R. C. & Harden, T. K. Mechanisms of Release of Nucleotides and Integration of Their Action as P2X–and P2Y–Receptor Activating Molecules. *Molecular Pharmacology* **64**, 785–795, https://doi.org/10.1124/mol.64.4.785 (2003).
6. Adriouch, S., Ohlrogge, W., Haag, F., Koch-Nolte, F. & Seman, M. Rapid Induction of Naive T Cell Apoptosis by Ecto–Nicotinamide Adenine Dinucleotide: Requirement for Mono(ADP–Ribosyl)Transferase 2 and a Downstream Effector. *The Journal of Immunology* **167**, 196–203 (2001).
7. Imai, S.-I. & Guarente, L. It takes two to tango: NAD+ and sirtuins in aging/longevity control. *Npj Aging And Mechanisms Of Disease* **2**, 16017, https://doi.org/10.1038/npjamd.2016.17 (2016).
8. Yoshino, J., Baur, J. A. & Imai, S.-I. NAD+ Intermediates: The Biology and Therapeutic Potential of NMN and NR. *Cell Metabolism* **27**, 513–528, https://doi.org/10.1016/j.cmet.2017.11.002 (2018).
9. Tullius, S. *et al.* NAD+ protects against EAE by regulating CD4+ T cell differentiation. *Nature Communications* **5**, 1–17, https://doi.org/10.1038/ncomms6101 (2014).
10. Elkhal, A. *et al.* NAD+ regulates Treg cell fate and promotes allograft survival via a systemic IL–10 production that is CD4+ CD25+ Foxp3+ T cells independent. *Scientific Reports* **6**, 22325, https://doi.org/10.1038/srep22325 (2016).

11. Stocchi, V., Cucchiarini, L., Magnani, M. & Fornaini, G. Adenine and pyridine nucleotides in the erythrocyte of different mammalian species. *Biochemistry International* **14**, 1043–1053 (1987).
12. Micheli, V. & Sestini, S. Determining NAD synthesis in erythrocytes. *Methods in Enzymology* **280**, 211–221, https://doi.org/10.1016/S0076-6879(97)80112-7 (1997).
13. O'Reilly, T. & Niven, D. F. Levels of nicotinamide adenine dinucleotide in extracellular body fluids of pigs may be growth–limiting for actinobacillus pleuropneumoniae and haemophilus parasuis. *Canadian Journal of Veterinary Research* **67**, 229–231 (2003).
14. Trammell, S. A. J. & Brenner, C. Targeted, LCMS–based Metabolomics for Quantitative Measurement of NAD(+) Metabolites. *Computational and Structural Biotechnology Journal* **4**, e201301012, https://doi.org/10.5936/csbj.201301012 (2013).
15. Liang, X. *et al*. Measuring NAD+ levels in mouse blood and tissue samples via a surrogate matrix approach using LC–MS/MS. *Bioanalysis* **6**, 1445–1457, https://doi.org/10.4155/bio.14.8 (2014).
16. Warburg, O., Christian, W. & Griese, A. Wasserstoffübertragendes Co–Ferment, seine Zusammensetzung und Wirkungsweise. *Biochem. z* **282**, 157–205 (1935).
17. Glock, G. & Mclean, P. The determination of oxidized and reduced diphosphopyridine nucleotide and triphosphopyridine nucleotide in animal tissues. *The Biochemical journal* **61**, 381–8, https://doi.org/10.1042/bj0610381 (1955).
18. Lowry, O., Passonneau, J., Schulz, D. & Rock, M. Measurement of Pyridine Nucleotides by Enzymatic Cycling. *The Journal of Biological Chemistry* **236**, 2746–2755 (1961).
19. H., C. P. Dosage des pyridine nucléotides oxydés et réduits dans le sang et les tissus animaux. *European Journal of Biochemistry* **4**, 247–255, https://doi.org/10.1111/j.1432-1033.1968.tb00201.x (1968).
20. Rhodes, M. & Wooltorton, L. A new fluorimetric method for the determination of pyridine nucleotides in plant material and its use in following changes in the pyridine nucleotides during the respiration climacteric in apples. *Phytochemistry* **7**, 337–353, https://doi.org/10.1016/S0031-9422(00)90872-0 (1968).
21. Woodley, C. & Gupta, N. New Enzyme Cycling Method for Determination of Oxidized and Reduced Nicotinamide Adenine Dinucleotide. *Analytical Biochemistry* **43**, 341–348, https://doi.org/10.1016/0003-2697(71)90262-4 (1971).
22. Jacobson, E. & Jacobson, M. Pyridine nucleotide levels as a function of growth in normal and transformed 3T3 cells. *Archives of Biochemistry and Biophysics* **175**, 627–634, https://doi.org/10.1016/0003-861(76)90553-1 (1976).
23. Bernofsky, C. & Swan, M. An improved cycling assay for nicotinamide adenine dinucleotide. *Analytical Biochemistry* **53**, 452–458, https://doi.org/10.1016/0003-2697(73)90094-8 (1973).
24. Zhu, C. T. & Rand, D. M. A Hydrazine Coupled Cycling Assay Validates the Decrease in Redox Ratio under Starvation in Drosophila. *PLoS ONE* **7**, e47584, https://doi.org/10.1371/journal.pone.0047584 (2012).
25. Lilius, E. M., Multanen, V. M. & Toivonen, V. Quantitative extraction and estimation of intracellular nicotinamide nucleotides of Escherichia coli. *Analytical Biochemistry* **99**, 22–27, https://doi.org/10.1016/0003-2697(79)90039-3 (1979).
26. Montero, M., Hernandez, J. & Estelrich, J. Fluorescence Quenching of Albumin. A spectrofluorimetric expermient. *Biochemical Education* **18**, 99–101, https://doi.org/10.1016/0307-4412(90)90188-T (1990).
27. Teale, F. The Ultraviolet Fluorescence of Proteins in Neutral Solution. *Biochemical Journal* **76**, 381–188 (1960).
28. Masilamani, V., Al-Zhrani, K., Al-Salhi, M., Al-Diab, A. & Al-Agiely, M. Cancer Diagnosis by Autofluorescence of Blood Components. *Journal of Luminescence* **109**, 143–154, https://doi.org/10.1016/j.jlumin.2004.02.001 (2004).
29. Madhuri, S. *et al*. Native Fluorescence Spectroscopy of Blood Plasma in the Characterization of Oral Malignancy. *Photochemistry and Photobiology* **78**, 197–204, 10.1562/0031-8655(2003)0780197NFSOBP2.0.CO2 (2003).
30. Lualdi, M. *et al*. Natural Fluorescence Spectroscopy of Human Blood Plasma in the Diagnosis of Colorectal Cancer: Feasibility Study and Preliminary Results. Tumorimmunology 567–571, https://doi.org/10.1177/030089160709300609 (2007).
31. Kalaivani, R. *et al*. Fluorescence Spectra of Blood Components for Breast Cancer Diagnosis. *Photomedicine and Laser Surgery* **26**, 251–256, https://doi.org/10.1089/pho.2007.2162 (2008).
32. Liu, Q., Kriksunov, I. A., Graeff, R., Hon, C. L. & Hao, Q. Structural Basis for Formation and Hydrolysis of the Calcium Messenger Cyclic ADP–Ribose by Human CD38. *Journal of Biological Chemistry* **282**, 5853–5861, https://doi.org/10.1074/jbc.M609093200 (2007).
33. Graeff, R. *et al*. Mechanism of cyclizing NAD to cyclic ADP–ribose by ADP–ribosyl cyclase and CD38. *Journal of Biological Chemistry* **284**, 27629–27636, https://doi.org/10.1074/jbc.M109.030965 (2009).
34. Sigma-Aldrich. β–Nicotinamide adenine dinucleotide, sodium salt from Saccharomyces cerevisae. Product number N7132. Datasheet (2003).
35. Lineweaver, H. & Burk, D. The determination of enzyme dissociation constants. *Journal of the American Chemical Society* **56**, 658–666, https://doi.org/10.1021/ja01318a036 (1934).
36. Dudka, J. *et al*. Effect of selected alcohol dehydrogenase inhibitors on human hepatic lactate dehydrogenase activity–an *in vitro* study. *Journal of Applied Toxicology* **25**, 549–553, https://doi.org/10.1002/jat.1094 (2005).
37. Lu, J., Stewart, A., Sadler, P., Pinheiro, T. & Blindauer, C. Albumin as a zinc carrier: properties of its high–affinity zinc–binding site. *Biochemical Society Transactions* **36**, 1317–1321, https://doi.org/10.1042/BST0361317 (2008).
38. Raj, S., Ramaswamy, S. & Plapp, B. Yeast Alcohol Dehydrogenase Structure and Catalysis. *Biochemistry* **53**, 5791–5803, https://doi.org/10.1021/bi5006442 (2014).
39. Berger, F., Lau, C., Dahlmann, M. & Ziegler, M. Subcellular compartmentation and differential catalytic properties of the three human nicotinamide mononucleotide adenylyltransferase isoforms. *Journal of Biological Chemistry* **280**, 36334–36341, https://doi.org/10.1074/jbc.M508660200 (2005).
40. Croce, A. C., Ferrigno, A., Santin, G., Vairetti, M. & Bottiroli, G. Bilirubin: An autofluorescence bile biomarker for liver functionality monitoring. *Journal of Biophotonics* **7**, 810–817, https://doi.org/10.1002/jbio.201300039 (2014).
41. Montejano, H. A., Gervaldo, M. & Bertolotti, S. G. The excited-states quenching of resazurin and resorufin by p-benzoquinones in polar solvents. *Dyes and Pigments* **64**, 117–124, https://doi.org/10.1016/0003-2697(89)90196-6 (2005).
42. Litt, M., Potter, J., Mezey, E. & Mitchell, M. Analysis of pyridine dinucleotides in cultured rat hepatocytes by high performance liquid chromatography. *Analytical Biochemistry* **179**, 34–36, https://doi.org/10.1016/0003-2697(89)90196-6 (1989).
43. Ryll, T. & Wagner, R. Improved ion–pair high–performance liquid chromatographic method for the quantification of a wide variety of nucleotides and sugar–nucleotides in animal cells. *Journal of Chromatography* **570**, 77–88, https://doi.org/10.1016/0378-4347(91)80202-N (1991).
44. Neves, A. R. *et al*. Is the glycolytic flux in lactococcus lactis primarily controlled by the redox charge? Kinetics of NAD+ and NADH pools determined *in vivo* by 13C NMR. *Journal of Biological Chemistry* **277**, 28088–28098, https://doi.org/10.1074/jbc.M202573200 (2002).
45. Anderson, R., Latorre-Esteves, M., Neves, A. & Lavu, S. Yeast life–span extension by calorie restriction is independent of NAD fluctuation. *Science* **302**, 2124–2126, https://doi.org/10.1126/science.1088697 (2003).
46. Sporty, J. L. *et al*. Single sample extraction protocol for the quantification of NAD and NADH redox states in Saccharomyces cerevisiae. *Journal of Separation Science* **31**, 3202–3211, https://doi.org/10.1002/jssc.200800238 (2008).
47. Yamada, K., Hara, N., Shibata, T., Osago, H. & Tsuchiya, M. The simultaneous measurement of nicotinamide adenine dinucleotide and related compounds by liquid chromatography/electrospray ionization tandem mass spectrometry. *Analytical Biochemistry* **352**, 282–285, https://doi.org/10.1016/j.ab.2006.02.017 (2006).

48. Formato, M., Masala, B. & De Luca, G. The levels of adenine nucleotides and pyridine coenzymes in red blood cells from the newborn, determined simultaneously by HPLC. *Clinica Chimica Acta* **189**, 131–137, https://doi.org/10.1016/0009-8981(90)90083-5 (1990).
49. Gentry, R. T. *et al*. Mechanism of the Aspirin-induced Rise in Blood Alcohol Levels. *Life Sciences* **65**, 2505–2512, https://doi.org/10.1016/S0024-3205(99)00517-2 (1999).
50. Caballería, J. *et al*. Effects of H2–Receptor Antagonists on Gastric Alcohol Dehydrogenase Activity. *Digestive diseases and sciences* **36**, 1673–1679 (1991).
51. Mezey, E. & Potter, J. J. Effects of Thyroidectomy and Triiodothyronine Administration on Rat Liver Alcohol Dehydrogenase. *Gastroenterology* **80**, 566–574 (1981).
52. Mezey, E., Potter, J. J. & Diehl, A. M. Depression of Alcohol Dehydrogenase Activity in Rat Hepatocyte Culture by Dihydrotestosterone. *Biochemical pharmacology* **35**, 335–339, https://doi.org/10.1016/0006-2952(86)90535-6 (1986).
53. Rachamin, G. *et al*. Modulation of Alcohol Dehydrogenase and Ethanol Metabolism by Sex Hormones in the Spontaneously Hypertensive Rat. Effect of Chronic Ethanol Administration. *Biochemical Journal* **186**, 483–490 (1980).
54. Stegink, L. D. *et al*. Blood Methanol Concentrations in Normal Adult Subjects Administered Abuse Doses of Aspartame. *Journal of Toxicology and Environmental Health, Part A Current Issues* **7**, 281–290, https://doi.org/10.1080/15287398109529979 (1981).
55. Dorokhov, Y. L. *et al*. Methanol may Function as a Cross-Kingdom Signal. *PLoS One* **7**, e36122 (2012).
56. Craft, N. E., Bulux, J., Valdez, C., Li, Y. & Solomons, N. W. Retinol Concentrations in Capillary Dried Blood Spots from Healthy Volunteers: Method Validation. *The American Journal of Clinical Nutrition* **72**, 450–454, https://doi.org/10.1093/ajcn/72.2.450 (2000).
57. Revollo, J. R., Grimm, A. A. & Imai, S.-I. TheNAD Biosynthesis Pathway Mediated by Nicotinamide Phosphoribosyltransferase Regulates Sir2 Activity in Mammalian Cells. *Journal of Biological Chemistry* **279**, 50754–50763, https://doi.org/10.1074/jbc.M408388200 (2004).
58. Scheuplein, F. *et al*. NAD+ and ATP Released from Injured Cells Induce P2X7–Dependent Shedding of CD62L and Externalization of Phosphatidylserine by Murine T Cells. *The Journal of Immunology* **182**, 2898–2908, https://doi.org/10.4049/jimmunol.0801711 (2009).
59. Bruzzone, S., Guida, L., Zocchi, E., Franco, L. & De Flora, A. Connexin 43 hemi channels mediate Ca2+–regulated transmembrane NAD+ fluxes in intact cells. *The FASEB Journal* **15**, 10–12, https://doi.org/10.1096/fj.00-0566.e (2000).
60. Balasubramaniyan, V. *et al*. Importance of Connexin–43 based gap junction in cirrhosis and acute–on–chronic liver failure. *Journal of Hepatology* **58**, 1194–1200, https://doi.org/10.1016/j.jhep.2013.01.023 (2013).
61. Fan, F., Lorenzen, J. A. & Plapp, B. V. An Aspartate Residue in Yeast Alcohol Dehydrogenase I Determines the Specificity for Coenzyme. *Biochemistry* **30**, 6397–6401, https://doi.org/10.1021/bi00240a008 (1991).
62. Lowry, O., Passonneau, J. & Rock, M. The stability of pyridine nucleotides. *The Journal of Biological Chemistry* **236**, 2756–2759 (1961).
63. Oyane, A. *et al*. Formation and growth of clusters in conventional and new kinds of simulated body fluids. *Journal of Biomedical Materials Research* **64**, 339–348, https://doi.org/10.1002/jbm.a.10426 (2003).

Acknowledgements

This work was supported by grants from the German Research Foundation (DFG, SCHM2661/3-1) and the Open Access Publication Fund of the Charité – Universitätsmedizin Berlin.

Author Contributions

P.B., A.L., F.K. and M.S. designed the study. P.B. and A.L. acquired the data. I.S., J.P. and M.S. were the principal physicians. P.H., G.A. and L.F. supervised patients and helped to acquire samples. C.K. and S.W. performed data cleaning. P.B., E.K., K.S. and K.K. ran statistical analyses. P.B., A.L., M.S. and F.K. prepared Figures. P.B. and A.L. drafted the manuscript and all authors reviewed the manuscript.

Additional Information

Supplementary information accompanies this paper at https://doi.org/10.1038/s41598-018-34350-6.

Competing Interests: The authors declare no competing interests.

Publisher's note: Springer Nature remains neutral with regard to jurisdictional claims in published maps and institutional affiliations.

PHILIPP MAXIMILIAN BRUNNBAUER

My curriculum vitae will not be published in this electronic version of my dissertation, due to data protection guidelines.

Mein Lebenslauf wird aus datenschutzrechtlichen Gründen in der elektronischen Version meiner Arbeit nicht veröffentlicht.

My curriculum vitae will not be published in this electronic version of my dissertation, due to data protection guidelines.

Mein Lebenslauf wird aus datenschutzrechtlichen Gründen in der elektronischen Version meiner Arbeit nicht veröffentlicht.

Appendix C

Acknowledgements

Above all, I would like to thank my incredible Family, *Hannah*, *Heike*, *Gerhard* and my grandparents, *Brigitte*, *Jürgen* and *Hilde* for always offering support when I needed it the most and for showing me what is truly important in life. You constantly inspire me to become a better version of myself. I wouldn't be here today if it wasn't for you.

Most importantly, I want to thank the the amazing medical director of the surgical clinic, *Prof. Dr. med. Johann Pratschke*, for planning and leaving me with this incredible project.

First and foremost, I would like to express my sincerest gratitude towards my two remarkable supervisors, *PD. Dr. med. Moritz Schmelzle* and *Dr. med. Felix Krenzien* who inspire me through their brilliance and bring out the best in me, always helping me get to the next stage. No matter the time of day, there were always there to answer my questions and help me out when I got stuck, thanks a million!

Without the help of my phenomenal colleague, *Dr. rer. nat. Annekatrin Leder* and her genius, this thesis wouldn't be possible and I am grateful for all her support and hard work she has dedicated to this project.

Likewise, I couldn't have done it without my good friend *Can Kamalı*, who has never shied away from hard work and has proven time and time again that he is extraordinary, both as a friend and as a colleague.

I would also like to thank *Kaan Kamalı* and *Helene Mayer* for contributing to this project and always giving valuable insights, as well as *Dr. med. Karl Hillebrandt* and *Assal Daneshgar* for generously aiding this project with their time and effort.

Thank you, my dear friends *Nicolas Mayer*, *Luna Haderer*, *Inès Borgel* and *Apolline Tosolini* for always making me laugh and reminding me that there is a life outside of the work bubble.

A special mention goes out to *Oscar Bian* for being an amazing flatmate and a truly exceptional friend, even in tough times, *Christian Mellor* for working incredibly hard to see our vision of a better healthcare system through and offering help when its needed most as well as *Alex Mellers* for always being incredibly and contagiously joyful and pushing me to be better.

In addition, I would like to thank the *MedEngine Team* who continue to surprise me with their motivation, brilliant ideas and spirits, making me more excited for the things to come.

Lastly, I would like to thank the team of Berlin Health Innovations, the technology transfer unit of the Charité - Universitätsmedizin Berlin, who, in collaboration with the Ascenion GmbH made it possible to file for a patent at the United States Patent and Trademark Office (USPTO) for the eNAD$^+$ assay.

Lastly I would like to extend my best wishes to the recent "junior members of staff" of *Dr. med. Felix Krenzien* and *Dr. rer. nat. Annekatrin Leder* and hope they will give you much joy in your life.